Heliyon 10 (2024) e38386

Contents lists available at ScienceDirect

Heliyon

journal homepage: www.cell.com/heliyon

Research article

Unraveling modulation effects on albumin synthesis and inflammation by Striatin, a bioactive protein fraction isolated from *Channa striata*: *In silico* proteomics and *in vitro* approaches

Affina Musliha [a,1], Doni Dermawan [a,1], Puji Rahayu [a], Raymond R. Tjandrawinata [a,b,*]

[a] *Dexa Laboratories of Biomolecular Sciences, PT Dexa Medica, Jababeka Industrial Estate II, Jl. Industri Selatan V Blok PP No. 7 Cikarang, 17550, Indonesia*

[b] *Faculty of Biotechnology, Atma Jaya Catholic University of Indonesia, South Jakarta 12930, Indonesia*

A R T I C L E I N F O

Keywords:
Hypoalbuminemia
NF-κB
Nucleoside diphosphate kinase
Parvalbumin
TGF-β

A B S T R A C T

Hypoalbuminemia, associated with inflammation in severely ill patients, can emerge due to decreased albumin production. Transforming growth factor-beta (TGF-β) and nuclear factor-kappa B (NF-κB) are critical signaling pathways responsible for decreased albumin expression. This study explores the protein content and modulation effects of Striatin on albumin synthesis and inflammation, employing *in silico* proteomics and *in vitro* investigations. In the *in silico* proteomics realm, LC/MS-MS protein sequencing, 3D modeling, protein-protein docking simulations, 100 ns molecular dynamics (MD) simulations, and MM/PBSA binding free energy calculations were carried out. Complementing this, *in vitro* studies examined Albumin gene expression and extracellular secretion in HepG2 cells subjected to lipopolysaccharides-induced hypoalbuminemia. Furthermore, the study probed Striatin's influence on the NF-κB expression, given albumin's role as a negative acute-phase protein. The results unveiled nucleoside diphosphate kinase (NdK) and parvalbumin (PV) as the prominent constituents within Striatin. Notably, NdK and PV exhibited the ability to disrupt hydrogen bonds with specific residues in both TGF-β and NF-κB complexes, thereby enhancing their flexibility, akin to the action of the FKBP12 complex (antagonist complex). In the *in vitro* experiments, Striatin demonstrated a dose and time-dependent inhibition of hypoalbuminemia, with peak efficacy observed at a concentration of

Abbreviations: 2-DE, two-dimensional gel electrophoresis; AA, arachidonic acid; ATCC, American type culture collection; BAPF, bioactive protein fraction; BLAST, basic local alignment search tool; CKD, chronic kidney disease; DHA, docosahexaenoic acid; ED, essential dynamics; HADDOCK, high ambiguity-driven protein-protein docking; IL-6, interleukin-6; I-TASSER, iterative threading assembly refinement; IPG, immobilized pH gradient; LC-MS/MS, liquid chromatography-tandem mass spectrometry; LPS, lipopolysaccharide; MD, molecular dynamics; MM/PBSA, molecular mechanics/poisson-boltzmann surface area; NCBI, national center for biotechnology information; Ndk, nucleoside diphosphate kinase; NF-κB, nuclear factor kappa β; NPT, number of particles, pressure, and temperature; NVT, number of particles, volume, and temperature; OPLS-AA/L, optimized potentials for liquid simulations; PCA, principal component analysis; PV, parvalbumin; Pvalb1, beta-1-parvalbumin; RMSD, root mean square deviations; RMSF, root mean square fluctuation; RoG, radius of gyration; SDS-PAGE, dodecyl sulfate-polyacrylamide gel electrophoresis; SPCE, single point charge extended; STR, short tandem repeat; TGF-β, transforming growth factor β; TNF-α, tumor necrosis factor-alpha; ULMW, ultra-low molecular weight.

* Corresponding author. Dexa Laboratories of Biomolecular Sciences, PT Dexa Medica, Jababeka Industrial Estate II, Jl. Industri Selatan V Blok PP No. 7 Cikarang, 17550, Indonesia.

E-mail address: raymond@dexa-medica.com (R.R. Tjandrawinata).

[1] Equal first authors.

https://doi.org/10.1016/j.heliyon.2024.e38386
Received 22 November 2023; Received in revised form 23 September 2024; Accepted 23 September 2024
Available online 24 September 2024

20 μg/mL. At this concentration, Striatin also suppressed NF-κB expression when co-incubated with lipopolysaccharides. While these findings suggest potential inhibitory effects of Striatin on TGF-β and NF-κB activities, they are preliminary and warrant further investigation. This study highlights Striatin's potential as a therapeutic agent for inflammation-related hypoalbuminemia, though additional research is needed to fully validate these results.

1. Introduction

Hypoalbuminemia is generally associated with inflammation in hospitalized and severely ill patients. Decreased albumin production, increased albumin catabolism, or increased loss of albumin through the kidneys, skin, and gastrointestinal tract are possible mechanisms that occur in the emergence of hypoalbuminemia [1]. Capillary permeability and release of serum albumin resulting from inflammation can increase the volume of albumin distribution, shorten the half-life of albumin, and decrease the total albumin mass [2]. Hypoalbuminemia can be an indicator of the severity of various diseases. For example, in chronic kidney disease (CKD), low serum albumin levels have been correlated with systemic inflammation, serving as a prognostic marker for higher mortality rates [3]. Similarly, research on colorectal cancer patients revealed a noteworthy association between hypoalbuminemia and increased systemic inflammatory response, indicating a heightened nutritional risk among this cohort [4]. In the realm of infectious diseases, particularly in the context of severe sepsis or septic shock, hypoalbuminemia often accompanies the inflammatory response. Research has demonstrated that low albumin levels in septic patients are associated with a higher likelihood of organ failure and increased mortality rates [5]. This emphasizes the role of hypoalbuminemia as an indicator of the severity of systemic inflammatory responses.

The cytokine that plays an essential role in the inflammatory response mediated by albumin expression is transforming growth factor β (TGF-β). This cytokine inhibits albumin production in normal human hepatocytes and hepatoma HepG2 cells by reducing albumin mRNA levels by 2-4-fold [6]. An *in vivo* study indicated that overexpression of TGF-β can trigger urinary albumin loss by increasing albumin permeability from the glomerulus [7]. Furthermore, increased levels of TGF-β are associated with loss of albumin in the body and increased levels of albumin in the urine (micro- and macroalbuminuria) through a lysosomal breakdown of albumin filtered by proximal tubular cells [8]. Besides TGF-β, nuclear factor kappa β (NF-κB) is vital in albumin expression. Lipopolysaccharide (LPS)-induced signaling activation and increased NF-κB activity decreased albumin expression dramatically [9]. This underscores the multifaceted nature of the inflammatory response and the involvement of various molecular pathways in modulating albumin levels. Considering the significance of TGF-β and NF-κB in albumin regulation, these cytokines emerge as potential targets for therapeutic intervention aimed at addressing hypoalbuminemia conditions. Inhibition of TGF-β and NF-κB pathways could hold promise in restoring normal albumin expression and mitigating the complications associated with altered albumin dynamics.

Nucleoside diphosphate kinase (Ndk) and parvalbumin (PV) are two proteins isolated from *Channa striata*, commonly known as the striped snakehead fish. *Channa striata* is a freshwater fish spread across Southeast Asian countries. This fish is a source of high-quality protein and is often used as a traditional medicine to treat various diseases [10]. Snakehead fish is used traditionally by local people to treat pain and wounds. It can also increase the energy and recovery of people with illnesses. Snakehead fish contains protein (more than 75 %), lipids, and vitamin A. It has a high content of docosahexaenoic acid (DHA) and arachidonic acid (AA), which help treat wounds and reduce inflammation [11,12]. Striatin is a form of development from *Channa striata* as a traditional medicine. It is a bioactive protein fraction isolated from snakehead fish that lives in Indonesian freshwaters. Striatin can accelerate wound healing and restore albumin levels in injured animal models [13]. Ndk is an enzyme involved in nucleotide metabolism associated with various biological functions, including cell signaling, DNA repair, and cell proliferation [14–16]. Parvalbumin, a low molecular weight calcium-binding protein, is known for its role in muscle relaxation and calcium homeostasis [17,18]. However, their potential therapeutic effects and molecular mechanisms of action in hypoalbuminemia have yet to be extensively investigated.

In recent years, *in silico* proteomics approaches have gained popularity in bioinformatics and drug discovery research. These computational methods allow researchers to analyze large-scale biological datasets and predict the interactions between proteins and potential drug compounds [19,20]. However, no integrative study has yet employed a combination of *in silico proteomics* and *in vitro* experimentation to investigate the therapeutic potential of *Channa striata* extract, leaving a gap in the comprehensive understanding of its molecular mechanisms and effects. Our study uniquely integrates *in silico* proteomics with *in vitro* experiments to address the existing research gaps. While prior research has largely focused on either computational or laboratory-based methods independently [21,22], our approach integrates both, enabling a more holistic understanding of Striatin's biological activity. Specifically, we employed *in silico* proteomics to characterize the molecular interactions and mechanisms of action of Striatin. The protein profile of Striatin was analyzed using two-dimensional gel electrophoresis (2-DE) and liquid chromatography-tandem mass spectrometry (LC-MS/MS). We further conducted molecular docking and molecular dynamics (MD) simulations (100 ns) to investigate how Striatin proteins interact with their target receptors (TGF-β and NF-κB). On the *in vitro* side, we explored how Ndk and PV affect the NF-κB expression. We assessed their effects on albumin synthesis in HepG2 cells under inflammatory conditions induced by LPS. This dual approach validates the computational predictions and reveals the molecular mechanisms by which Striatin modulates inflammation and restores albumin levels. By bridging computational and experimental methods, our study advances current knowledge of the therapeutic applications of bioactive proteins derived from *Channa striata*. This integrated approach offers a robust framework for exploring Striatin's potential in managing hypoalbuminemia and inflammation, providing a foundation for future translational research and clinical applications.

2. Materials and methods

2.1. Striatin bioactive fraction

Striatin was obtained and developed at Dexa Laboratories Biomolecular Science (DLBS), PT Dexa Medica, Cikarang, Indonesia. Striatin is a bioactive protein fraction (BAPF) from *Channa striata* fillet meat from freshwater waters in West Java, Indonesia. This BAPF was obtained by extracting *Channa striata* using a water-based solvent and then processed through a multi-step fractionation, concentration, and drying process.

2.2. Computing power

The employed computing power for the *in silico* proteomics approach in this study was a workstation that has the following specifications: Intel® Core™ i9-10900K CPU @3.70Ghz x 20, NVIDIA GeForce RTX 3090 24 GB, RAM 32 GB DDR5, HDD 4 TB, and Ubuntu operating system.

2.3. Proteomics study of striatin

To identify the proteins present in Striatin, a 2-DE technique was used. This technique separates proteins based on their isoelectric point and molecular weight. Subsequently, LC-MS/MS was employed to identify the proteins from the 2-DE gels. This approach allowed us to characterize the protein composition of Striatin.

2.3.1. Protein separation by gel electrophoresis

The protein profile of Striatin was analyzed by gradient 10 % and 16.5 % Tricine sodium dodecyl sulfate-polyacrylamide gel electrophoresis (SDS-PAGE), using ultra-low molecular weight markers (1.02–26.6 kDa). In addition, protein bands were visualized by Coomassie Brilliant Blue R-250 [23]. 2-DE also separated the proteins present in Striatin, using a wide range of immobilized pH gradient (IPG) strips (pH 3–10). Striatin (equal to 200 μg of protein) was diluted using rehydration buffer (urea 8 M, CHAPS 2 %, Dithiothreitol 50 mM, Bio-Lyte 0.2 %, and bromocresol blue). The IPG strip rehydration was done by diluting the Striatin solution in a rehydration/equilibration tray for 16 h at 4 °C. In the first dimension, the separation was conducted through three different voltages: 250 V for 20 min, 400 V for 2 h, and 10,000 V for 4 h. After the first dimensional electrophoresis, the IPG strip was run on gradient Tricine SDS-PAGE. Protein spots were then visualized by Coomassie Brilliant Blue R-250 staining.

2.3.2. Protein digestion, mass spectrometry, and database searching

All protein spots were manually excised from the 2-DE, stored at 4 °C for further analysis, and were sent to Proteomics International; Pty. Ltd. (Broadway, Nedlands, Australia) for protein identification. Firstly, the individual protein was digested in the trypsinized gel. Then, the digested products were extracted according to the standard techniques before LC-MS/MS analysis [24]. Extracted peptides with molecular weights around 10.9, 8.3, 15.4, and 16.7 kDa were individually analyzed using an LC-MS/MS, the Agilent 1260 Infinity HPLC system (Agilent), coupled to an Agilent 6540 mass spectrometer (Agilent) (LC-MS/MS). Tryptic peptides were loaded onto a C18 column 300 SB, 5 μm (Agilent), and separated with a linear gradient of water/acetonitrile/0.1 % (v/v) formic acid. Each spectrum was analyzed with Mascot sequence matching software (Matrix Science) using the MSPnr100 database (for LC-MS/MS) to identify the protein of interest. Each peptide ion data fragmented within the mass spectrometer was matched to the possible amino acid sequences in the database. Furthermore, the resulting sequences were then searched against the National Center for Biotechnology Information (NCBI) protein database using the basic local alignment search tool (BLAST) to provide the sequence coverage of Striatin's peptides in each spot to the predicted protein. Blast analysis was subsequently conducted and followed by sequence alignment (http://www.ebi.ac.uk/Tools/services/web).

2.4. In silico study of striatin

In addition to the experimental characterization, *in silico* protein-protein interaction studies were conducted to investigate the interactions between proteins from Striatin and their potential target molecules, specifically TGF-β and NF-κB. *In silico* methods, such as molecular docking, were employed to predict and to analyze the binding interactions between Striatin proteins and the target receptors. Furthermore, MD simulations, lasting 100 ns (ns), were performed to study the dynamic behavior and stability of the protein-protein complexes formed between Striatin and its target receptors. These simulations allow the researchers to observe the conformational changes and intermolecular interactions over an extended period.

2.4.1. 3D structure modeling

The nucleoside diphosphate kinase (Ndk) and parvalbumin (PV) as the two major proteins (based on % sequence coverage) of Striatin were chosen for *in silico* study. Briefly, the 3D model structures of Ndk (PDB template: 4UOF [25]) and PV (PDB template: 5ZGM [26]) were built by employing iterative threading assembly refinement (I-TASSER) [27] based on the matched protein sequences.

2.4.2. Protein-protein docking simulation

We investigated the intermolecular interactions of Ndk and PV isolated from Striatin with their target receptors (TGF-β and NF-κB). Protein-protein docking simulations determined key residues responsible for forming protein-protein complexes, types of intermolecular interactions, binding affinities, binding modes, and orientations. To obtain information regarding the binding site of TGF-β (PDB ID: 1B6C [28]) and NF-κB (PDB ID: 1SVC [29]), the protein-protein interactions were analyzed using PDBSum [30]. The advanced interface option in the High Ambiguity Driven Protein-Protein Docking (HADDOCK) stand-alone version [31] was used to perform protein-protein docking calculations for the Ndk and PV against TGF-β and NF-κB. The best protein-protein docking results for each resulting complex were selected based on two essential criteria: (1) the most significant number of clusters or populations and (2) the highest docking score (HADDOCK score), which indicates the strongest binding affinity between the two proteins in the protein-protein complex. Furthermore, the intermolecular interactions in the protein complexes were determined using Protein Interactions Calculator (PIC) with default parameters [32].

2.4.3. Molecular dynamics (MD) simulation

Molecular dynamics (MD) simulations were performed for the generated protein–protein complexes employing GROMACS 2022.5 [33]. The Optimized Potentials for Liquid Simulations (OPLS-AA/L) all-atom force field and the default cubic box parameters were used to set up the MD simulations [34]. Several standard steps were followed, including the preparation of input files, the definition of the box dimensions, the addition of water molecules using Single Point Charge Extended (SPCE), and the inclusion of counterions to neutralize the system. The energy minimization phase was carried out using the steepest-descent approach, followed by a two-phase equilibration process including phase 1: Number of particles, Volume, and Temperature (NVT) ensemble; and phase 2: Number of particles, Pressure, and Temperature (NPT) ensemble to stabilize the system. Subsequently, production MD simulations were performed for 100 ns for the protein-protein complexes. The GROMACS package provided various built-in functions to analyze the simulation results, such as Root Mean Square Deviations (RMSD), Root Mean Square Fluctuation (RMSF), Radius of Gyration (RoG), potential energies, and intermolecular hydrogen bonding interactions. To visualize the crucial residues and intermolecular interactions within the predicted protein-protein complex, a manual inspection was performed using the PyMOL program [35].

2.4.4. Molecular Mechanics/Poisson–Boltzmann Surface Area (MM/PBSA) calculations

The Molecular Mechanics/Poisson-Boltzmann Surface Area (MM/PBSA) calculation method, based on MD simulations, was utilized to examine the protein-protein interactions involved in downregulating TGF-β and NF-κB overexpression by Ndk and PV from Striatin (*Channa striata*) under hypoalbuminemia conditions. MD simulations generated an ensemble of protein conformations and selected representative snapshots. Gas-phase energy calculations, solvation energy estimations using a continuum solvent model, and entropy calculations were performed for each snapshot. The binding free energy was then computed by combining these contributions. The *gmx_MMPBSA* module from GROMACS was employed to perform the calculations [36,37]. The MM/PBSA method is commonly used to predict the binding free energy of a protein-protein complex [38]. The equation for calculating the MM/PBSA binding free energy is as follows:

$$\Delta G\_binding = \Delta G\_complex - \Delta G\_protein1 - \Delta G\_protein2$$

Where:

ΔG_binding is the binding free energy of the protein-protein complex.

ΔG_complex is the free energy of the fully solvated protein-protein complex.

ΔG_protein1 is the free energy of protein 1 in its solvated state (unbound).

ΔG_protein2 is the free energy of protein 2 in its solvated state (unbound).

The binding free energy is estimated by computing the difference between the free energy of the complex and the sum of the individual free energies of the unbound proteins. This accounts for the energetic changes that occur upon complex formation.

2.5. In vitro study of striatin

The *in vitro* experiments aimed to assess the expression of the albumin gene and the release of Albumin into the extracellular environment in HepG2 cells induced with hypoalbuminemia caused by lipopolysaccharides. Furthermore, the study investigated how Striatin influenced the total NF-κB expression, taking into account the fact that albumin acts as a negative acute-phase protein.

2.5.1. Protein content assay

Protein concentration was quantified using the Bradford method. Sample (100 μL) was added to 2 mL of Bradford reagent (100 mg Coomassie G250 (Sigma-Aldrich), 50 mL of ethanol 95 % (Sigma-Aldrich), 100 mL of phosphoric acid 85 % (Sigma-Aldrich), and water up to 1 L volume. The mixture was incubated for 10 min at room temperature, and the absorbance was measured at 595 nm. The standard curve was prepared using BSA fraction V (Merck, Germany) at various concentrations to determine Striatin protein concentration during cell treatment.

2.5.2. Cell line reporting requirements and cell viability assay

Cell viability was assessed using the human hepatocellular carcinoma cell line HepG2 (ATCC, HB-8065, RRID: CVCL_0027). These cells were obtained from the American Type Culture Collection (ATCC) and authenticated using short tandem repeat (STR) profiling to

confirm their identity. Additionally, they were tested and found negative for mycoplasma contamination. The HepG2 cells were cultured in Minimum Essential Medium (MEM) supplemented with 10 % fetal bovine serum (FBS) and 1 % penicillin-streptomycin (PS) and maintained under standard culture conditions. For the cell viability assay, HepG2 cells were seeded in 96-well plates and treated with various concentrations of Striatin (0–500 μg/mL) for 24 h. After the treatment period, cell viability was assessed using the 3-(4,5-dimethylthiazol-2-yl)-2,5-diphenyltetrazolium bromide (MTT) assay according to the manufacturer's instructions (Promega, Madison, Wi, USA). MTT is a colorimetric assay that measures the reduction of MTT by viable cells to form insoluble formazan crystals, providing an indirect measure of cell viability. To ensure reproducibility, each condition was tested in triplicate within each experiment, and the assay was performed across three independent experiments.

2.5.3. Optimization of LPS-induced decrease in albumin secretion

Before treatment, the HepG2 cells were seeded at a density of 10×10^4 cells per well in a 6 mm cell culture dish (Iwaki) and incubated in a complete medium for 2 h before use (3 replicates in each group). Cells were incubated in a serum-free medium for another 24 h to diminish serum in the medium completely. Afterward, cells were exposed to LPS at various concentrations (0–1000 ng/mL) for 24 h to obtain optimal conditions for LPS-induced reduction in albumin secretion. Subsequently, HepG2 cells were incubated with an optimal concentration of LPS at four different incubation times (24, 48, 72, and 96 h). The total mRNA and extracellular proteins were isolated for further assay.

2.5.4. Treatment of Striatin on LPS-induced decrease in albumin secretion HepG2 cell line

After reaching confluency, HepG2 cells were incubated (3 replicates in each group) with the optimal LPS concentration, then co-incubated with Striatin at various concentrations (0–40 μg/mL) at three different times (24, 48, and 72 h). To ensure that fluctuations in cell viability did not affect the results, controls were included at each time point (24, 48, and 72 h) to provide a basis for comparison and to validate the continued viability of the cells throughout the experiment. Total mRNA and extracellular protein were analyzed to investigate the effect of Striatin on LPS-induced suppression of albumin secretion. Human serum albumin (HSA, CSL Behring), with a concentration of 10 μg/mL, was used as a comparator.

2.5.5. Total mRNA isolation and reverse transcriptase polymerase chain reaction (RT-PCR)

Total mRNA was isolated using TRIzol reagent (Invitrogen) and then processed using RT-PCR to obtain cDNA. Total mRNAs (1 μg) were added to 10 μL of reaction mixture containing 2 μL of Reverse Transcriptase buffer, 0.5 μL of Reverse Transcriptase Enzyme Mix, and 0.5 μL of primer mix from ReverTra Ace™ qPCR RT Kit (Toyobo). The cDNA was subjected to RT-PCR to determine albumin and nuclear factor kappa B (NF-κB) gene expression. PCR was performed with 2 μL of cDNA in 20 μL of reaction mixture containing 10 μL of Ssofast™ Evagreen® MasterMix (Biorad), and 1 μL of 5 μM each sense and antisense primers. The glyceraldehyde 3-phosphate dehydrogenase (GAPDH) was used as the internal control for the RT-PCR reaction. Relative gene expressions were calculated using the ΔΔCq method relative to untreated control in 24 h of treatment. The PCR primer sequences and obtained product sizes for gene amplification are provided in Table 1.

2.5.6. Enzyme-linked immunosorbent assay (ELISA)

The expression of HSA was measured with sandwich ELISA using a specific antibody (Santa Cruz, USA; Abcam, USA). A 96-well plate (Greiner Bio-one 705070) was coated overnight with 100 μL of 1 μg/μL anti-HSA (Abcam, [15C7] Ab2406). Wells were washed three times with 200 μL of washing buffer (twice with phosphate-buffered saline (PBS), once with 200 μL of tris-buffered saline, 0.1 % Tween® 20 detergent (TBST)). Blocking was conducted using 150 μL of 2.5 % BSA (Sigma, USA) in PBS for 1 h at room temperature with gentle shaking. Antigen solution (50 μL) was loaded and incubated for 1 h at room temperature. The wells were rewashed three times, and an amount of 0.5 μg/mL detection antibody was added (Anti-HSA Ab2406, Abcam). After a similar procedure of incubation and washing, wells were incubated with 100 μL of secondary antibody-tagged horseradish peroxide (HRP) (1:1000) (Santa Cruz, USA) in blocking solution for 1 h at room temperature with gentle shaking. The color was developed by adding 50 μL of TMB (Sigma, USA), stopped by 0.25 M of sulfuric acid solution, and the absorbance was measured at 450 nm. The standard absorbance calibration curve was generated using native HSA (Abcam). Extracellular HSA relative quantity was calculated by normalizing the albumin content of each sample to control.

2.5.7. Statistical analysis

The data were presented as mean ± SD (standard deviation). Data analysis was performed using SPSS ver. 22.0 (IBM Corp, Armonk,

Table 1
PCR primer sequences and product sizes for gene amplification in hypoalbuminemia study.

Gene	Primer	Sequence (5' - 3')	Product size (bp)
Albumin (ALB)	Forward	TGCTTGAATGTGCTGATGACAGGG	162
	Reverse	AAGGCAAGTCAGCAGGCATCTCAT	
Nuclear factor kappa b subunit (NFkB)	Forward	GCTTAGGAGGGAGAGCCCAC	107
	Reverse	AACATTTGTTCAGGCCTTCCC	
Glyceraldehyde 3-phosphate dehydrogenase (GAPDH)	Forward	ATGACAACAGCCTCAAGATCATCAG	607
	Reverse	CTGGTGGTCCAGGGGTCTTACTCCT	

NY, USA). One-way analysis of variance (ANOVA) followed by the Tukey post hoc test was used to analyze samples. The value of $p < 0.05$ was considered a significant difference between the tested groups.

3. Results

3.1. Proteomics study of striatin

The protein analysis conducted on Striatin revealed a protein profile consisting of four distinct protein bands with molecular weights ranging from 6.5 to 17 kDa (Fig. 1a). This initial characterization provided an overview of the protein components in the Striatin sample. To further investigate the protein composition, a 2-DE analysis was performed. The four protein bands observed in the protein profile were separated into seven distinct protein spots on the 2-DE gel (Fig. 1b). Each protein spot represented a protein with a specific molecular weight and isoelectric point (pI). The 2-DE analysis revealed three spots with molecular weights around 10.9 kDa, two spots at approximately 8.3 kDa, and the remaining spots at about 15.4 and 16.7 kDa, respectively. Significantly, all protein spots fell within the pH range of 4–10, indicating their isoelectric points.

To identify the proteins corresponding to these spots, LC-MS/MS analysis was performed. The results of the LC-MS/MS analysis, including the protein hits and the number of matched peptides for each spot, were summarized in Table 2. Mascot sequence query analysis revealed that spots S1 and S2 were identified as nucleoside diphosphate kinase (Ndk), while spots S3, S4, and S5 were similar to parvalbumin (PV). Additionally, spots S6 and S7 were identified as beta-1-parvalbumin (Pvalb1). Identifying the proteins was based on comparing the amino acid sequences of peptides obtained from each spot with those of known protein hits. The percentage of sequence coverage from all matched peptides to the mature peptide of the predicted protein was also considered during the identification process. These findings hold significance for understanding the protein components of Striatin. The presence of Ndk, PV, and Pvalb1 indicates their potential involvement in the biological processes associated with Striatin. However, Pvalb1 was not included in the *in silico* study because Pvalb1 has a protein sequence similar to PV (higher % coverage).

3.2. In silico study of striatin

In this *in silico* study, the protein-protein interactions and binding free energy were investigated through a series of computational methods. The process involved constructing 3D models of the proteins, performing protein-protein docking simulations to predict binding orientations, conducting MD simulations to simulate complex dynamics, and finally estimating the binding free energy using the MM/PBSA approach. These techniques allowed for a comprehensive analysis of the protein-protein interactions, providing insights into their binding modes, dynamics, and energetics.

3.2.1. 3D model construction

In this research, the 3D model structures of nucleoside diphosphate kinase (Ndk) and parvalbumin (PV) from Striatin were constructed using I-TASSER, a widely used computational method for protein structure prediction [27]. The modeling process involved aligning the protein sequences of Ndk and PV with templates available in the Protein Data Bank (PDB), ensuring the reliability of the generated models. The nucleoside diphosphate kinase fragment of Striatin was successfully modeled in 3D using molecular simulation techniques. At the same time, the coverage percentage from the sequencing results indicated that the resulting 3D structure was incomplete (49.66 % coverage). The 3D modeling analysis provided insights into the active site of nucleoside diphosphate kinase from

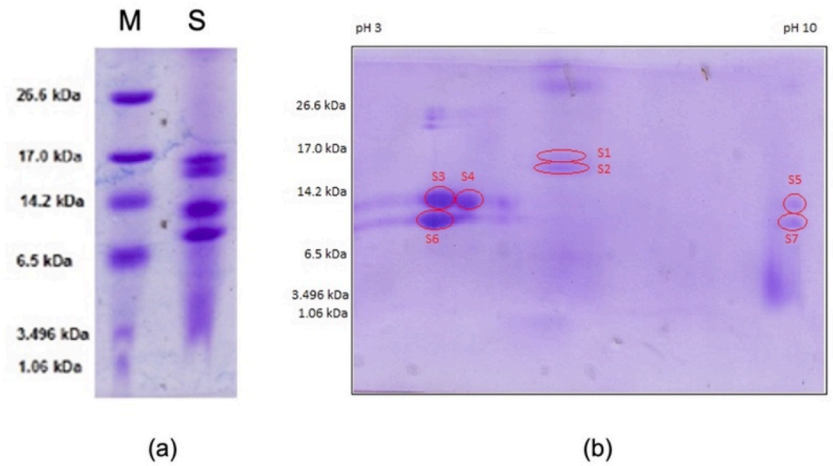

Fig. 1. Striatin protein profile analysis using two-dimensional gel electrophoresis and Tricine-SDS PAGE. (a) Tricine-SDS PAGE gel showing the separation of proteins. Lane M: Ultra-low molecular weight (ULMW) protein marker, Lane S: Striatin sample. (b) 2D-Electrophoresis image highlighting protein spots corresponding to Striatin.

Table 2
Peptide information and amino acid sequence alignment of Striatin's spot.

Protein spot	Protein size (MW, kDa)	Matched peptide	Peptide score	Amino acid sequence	Sequence coverage (%)	Annotation
S1	15.4	25	320	1 ME**RTFIAVKP DGVQRG**LCGD IIKRFEQRGF RLVAAKFMQA SDDHM**KKHYL DLKDK**PFYAG 61 LC**KYMSSGPI LAMVWEGQNI VKL**ARMMLGE TNPADSKPGS IRGDLCIDIG RNIIHGSDTV 121 ENA**KTEVDLW FKA**EEFVSYT PCAQPFLYE	49.66	Nucleoside diphosphate kinase
S2	16.7	55	1110	1 ME**RTFIAVKP DGVQRGLCGD IIKRF**EQRGF RLVAA**KFMQA SDDHMKKH**YL DLKDKPFYAG 61 LC**KYMSSGPI LAMVWEGQNI VKLARMMLGE TNPADSKPGS IRGDLCIDIG RNIIHGSDTV** 121 **ENAKTEVDLW FKA**EEFVSYT PCAQPFLYE	45.64	Nucleoside diphosphate kinase
S3	10.9	41	1160	1 MAFAGVLKDA DITAALEAC**K AADSFNYKA**F FAKVGLSNKS PDDI**KKAFSI IDQDKSGFIE** 61 **EDELKLFLQN F**SKGARALTD KETKAFLQ**AG DTDGDGKIG**I DEFAAVVKA	44.04	Parvalbumin
S4	10.9	41	481	1 MAFAGVLKDA DITAALEAC**K AADSFNYKA**F FAKVGLSNKS PDDIK**KAFSI IDQDKSGFIE** 61 **EDELKLFLQN F**SKGARALTD KETKAFLQ**AG DTDGDGKIG**I DEFAAVVKA	43.12	Parvalbumin
S5	10.9	41	464	1 MAFAGVLKDA DITAALEAC**K AADSFNYKA**F FAKVGLSNKS PDDI**KKAFSI IDQDKSGFIE** 61 **EDELKL**FLQN FSKGARALTD KET**KAFLQAG DTDGDGKIG**I DEFAAVVKA	43.12	Parvalbumin
S6	8.3	64	1738	1 MAFSNVLSDS DVAAALDGCK DAGTFDHKKF FSACGLSNKT SDD**VKKAFAI IDQDKSGFIE** 61 **EEELKLFLQN F**KADARVLTD VETST**FLKAG DTDGDGKIG**A DEFTALVKP	37.61	Beta-1-Parvalbumin
S7	8.3	63	294	1 MAFAGILNEA DITAALAACQ AADSFKHKDF FVKVGLAGKS DDDV**KKAFAV IDQDKSGFIE** 61 **EDELKLFLQN FSASARA**LTD AET**KEFLKAG DSDGDGKIG**V DEFAALVKV	44.03	Beta-1-Parvalbumin

Bold = Identified peptide fragments from LC-MS/MS Analysis.

Striatin (Fig. 2a). The active site was identified to be composed of specific amino acid residues, including Lys 7, Leu 22, Lys 25, Lys 26, and Tyr27 (Fig. 2b). Understanding the composition and arrangement of these residues offers important clues regarding the functional mechanisms of Ndk within the context of Striatin. Furthermore, the 3D modeling process sheds light on the structural characteristics of Ndk, which are essential for its interaction with target molecules such as TGF-β and NF-κB. By identifying key residues within the active site, we gain insights into the potential binding interfaces and interaction modes between Ndk and its targets. This information is crucial for elucidating the molecular mechanisms underlying the therapeutic effects of Striatin.

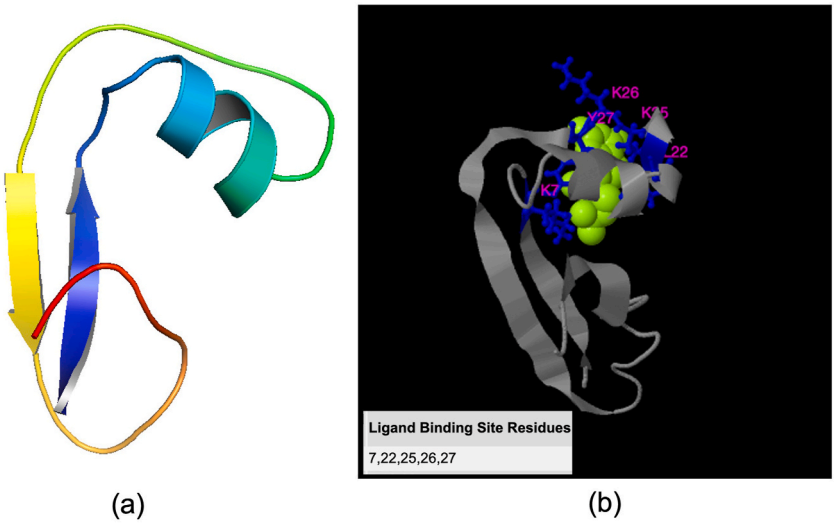

Fig. 2. Molecular modeling of nucleoside diphosphate kinase (Ndk) from Striatin. (a) 3D structural model of Ndk highlighting key structural features. (b) Identification of binding site residues critical for protein-protein interactions.

In a similar vein, we employed molecular simulation techniques to construct a 3D model of the Parvalbumin fragment found in Striatin. Despite encountering challenges with incomplete coverage, as indicated by a 44.04 % coverage rate based on sequencing results, we successfully generated a 3D structure of Parvalbumin. This modeling analysis provided valuable insights into the structural characteristics of Parvalbumin and its potential functional implications within Striatin. The 3D modeling analysis of Parvalbumin revealed the presence of an active site composed of specific amino acid residues (Fig. 3a). Among these residues are Asp 18, Asp 20, Ser 22, Phe24, Glu26, and Glu 29 (Fig. 3b). Importantly, these interactions are crucial for Parvalbumin's biological function within the context of Striatin. Of particular significance is the role of these amino acid residues in mediating interactions with key molecular targets, such as TGF-β and NF-κB. Both TGF-β and NF-κB are central players in cellular expressions implicated in inflammation and immune response regulation. The identification of specific residues within the active site of Parvalbumin highlights its potential involvement in modulating these expressions through protein-protein interactions. By elucidating the structural features of Parvalbumin and its interaction interfaces, we gain valuable insights into its molecular mechanisms of action within the complex network of biological processes regulated by Striatin. Understanding the intricate details of Parvalbumin's structure-function relationships is essential for unraveling its therapeutic potential and developing targeted interventions for conditions associated with inflammation and immune dysregulation.

3.2.2. Protein-protein docking simulation

The protein-protein docking simulations between nucleoside diphosphate kinase (Ndk) and parvalbumin (PV) with TGF-β and NF-κB were conducted using the HADDOCK stand-alone version [31]. In addition, FKBP12 was included in the simulations as the standard inhibitor. FKBP12, a protein known as FK506-binding protein 12, has been found to play a crucial role in inhibiting TGF β receptor-mediated signaling [39–41]. The HADDOCK provides an easy interface option for performing these docking simulations, which are crucial for understanding the molecular interactions between the proteins. To select the most promising docking solutions for each protein-protein complex, two critical criteria were considered. Firstly, the number of populations or docking solutions in the largest cluster was examined. A higher number of populations suggests a higher likelihood of biologically relevant complex formations. This criterion helps identify the most dominant and stable docking solutions. Secondly, the docking or HADDOCK score was assessed to evaluate the binding affinity between the two proteins in the complex. A higher docking score indicates a stronger interaction and a more favorable binding between the proteins.

To gain insights into the binding site of TGF-β (PDB ID: 1B6C [42]) and NF-κB (PDB ID: 1SVC [43]) within the protein-protein complex, further analysis was performed using PDBSum [30]. PDBSum is a valuable resource that provides detailed information about protein structures and their interactions. By utilizing PDBSum, we can identify the specific regions or residues within Ndk and parvalbumin that could interact with TGF-β and NF-κB. This information is crucial for understanding the molecular basis of the protein-protein interaction and can offer insights into the functional implications of the complex formation.

The results of the protein-protein docking simulations revealed that all three protein complexes, namely TGF-β:FKBP12 (Fig. 4a), TGF-β:Ndk (Fig. 4b), and TGF-β:PV (Fig. 4c), exhibited interactions in similar binding regions. However, the TGF-β:FKBP12 complex displayed the lowest docking score (−158.0 kcal ±2.1) and free energy of binding (−11.1 kcal/mol), indicating a stronger and more favorable binding affinity compared to the TGF-β:Ndk (−91.4 ± 9.5; −10.1 kcal/mol) and TGF-β:parvalbumin (−83.3 ± 2.0; −10.3 kcal/mol) complexes. This finding suggests that FKBP12, serving as a standard inhibitor, has a higher propensity to bind to TGF-β compared to Ndk and PV from Striatin. The lower binding score implies that FKBP12 binds more easily and exhibits a stronger interaction with TGF-β, potentially leading to more efficient inhibition of TGF-β-mediated signaling. Interestingly, both Ndk and PV complexes exhibited a similar hydrogen bond formation with the Asn 267 residue of TGF-β. This suggests that Ndk and PV have the

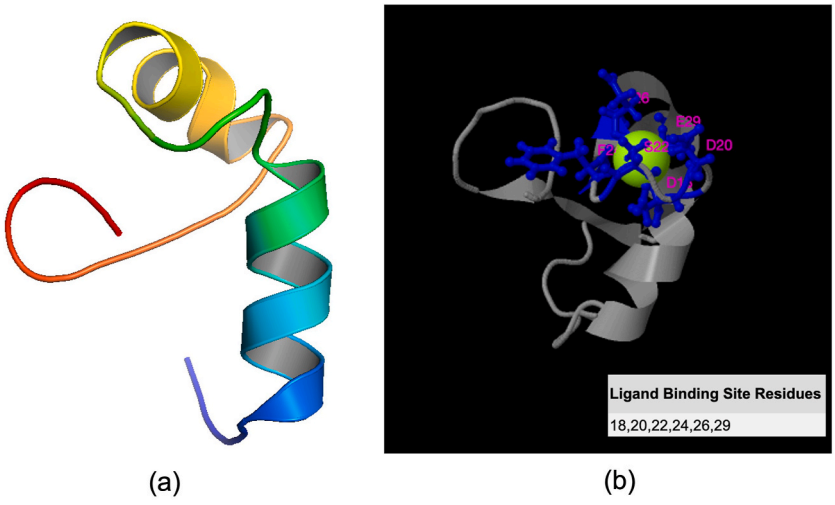

Fig. 3. Molecular modeling of Parvalbumin from Striatin. (a) 3D structural model of Parvalbumin (PV) highlighting key structural features. (b) Identification of binding site residues critical for protein-protein interactions.

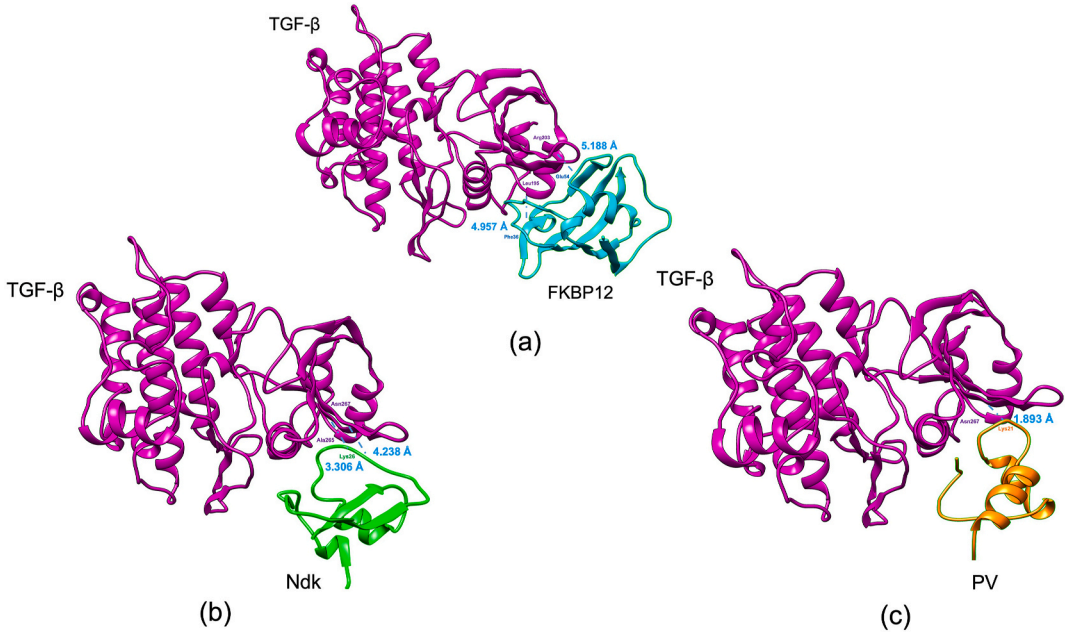

Fig. 4. Predicted protein-protein complexes obtained from docking simulations illustrating the interactions between Striatin and TGF-β. (a) Docked structure of FKBP12 bound to TGF-β, (b) Docked structure of nucleoside diphosphate kinase (Ndk) interacting with TGF-β, and (c) Docked structure of Parvalbumin (PV) forming a complex with TGF-β.

potential to inhibit the activity of TGF-β by adopting a binding pose similar to FKBP12.

Similar to TGF-β complexes, the NF-κB:FKBP12 (Fig. 5a), NF-κB:Ndk (Fig. 5b), and NF-κB:PV (Fig. 5c), exhibited interactions in similar binding regions, suggesting potential interactions between these proteins. Notably, the NF-κB:Ndk complex displayed similar docking score (102.3 ± 7.1) and free energy of binding (-11.1 kcal/mol) compared to the NF-κB:FKBP12 complex, which has docking score of -102.3 ± 7.6 and free energy of binding -11.0 kcal/mol. This indicates that NF-κB forms a stable complex with Ndk, similar to its complex with FKBP12 (a standard inhibitor). The similar binding energy suggests that Ndk has a comparable binding affinity to

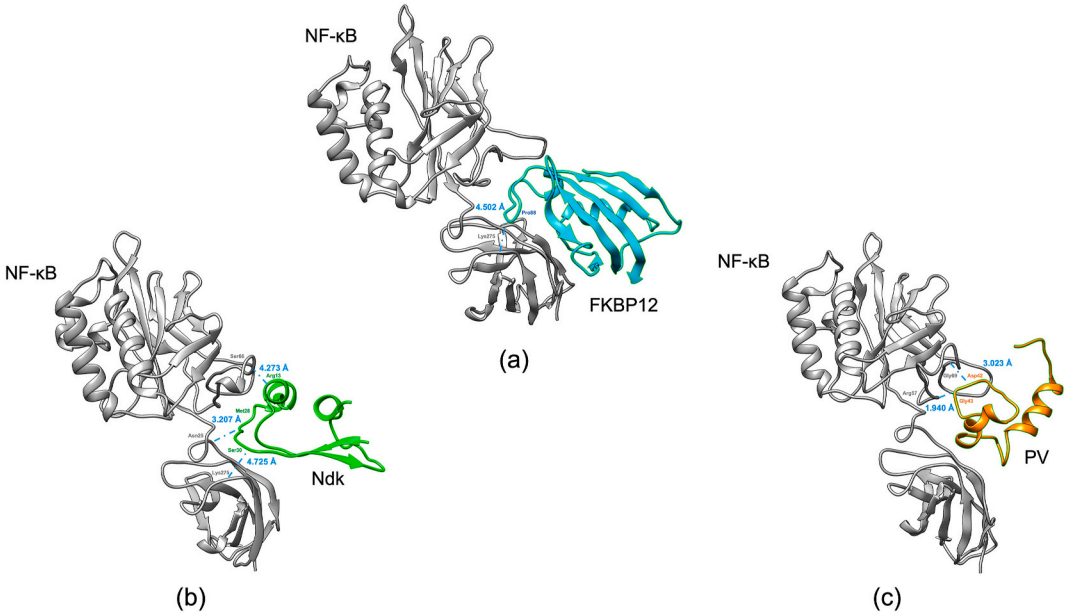

Fig. 5. Predicted protein-protein complexes obtained from docking simulations illustrating the interactions between Striatin and NF-κB. (a) Docked structure of FKBP12 bound to NF-κB, (b) Docked structure of nucleoside diphosphate kinase (Ndk) interacting with NF-κB, and (c) Docked structure of Parvalbumin (PV) forming a complex with NF-κB.

NF-κB as FKBP12, making it a potential inhibitor of NF-κB activity. Interestingly, the Ndk and parvalbumin complexes formed more hydrogen bonds with NF-κB compared to FKBP12. Hydrogen bonds play a crucial role in stabilizing protein-protein interactions and can contribute to the strength and specificity of binding [44]. The increased number of hydrogen bonds observed in the Ndk and parvalbumin complexes suggests a more favorable binding interaction with NF-κB compared to FKBP12. Based on these results, it can be inferred that Ndk and parvalbumin have the potential to inhibit the activity of NF-κB, similar to the effect of FKBP12. Their binding poses, which resemble that of FKBP12, enable them to interact with NF-κB and potentially modulate its signaling activity. These findings highlight the promising inhibitory capabilities of Ndk and parvalbumin on NF-κB activity. The details of binding affinities, energy parameters, and interface characteristics of the protein-protein complexes can be seen in Table 3.

Table 4 provides an analysis of the intermolecular interactions in the protein-protein complexes, focusing on hydrophobic interactions, main chain-main chain hydrogen bonds, main chain-side chain hydrogen bonds, side chain-side chain hydrogen bonds, ionic interactions, and cation-pi interactions. In the TGF-β complexes, TGF-β:FKBP12 demonstrates the highest number of hydrophobic interactions, with 15 observed. It also shows significant contributions from side chain-side chain hydrogen bonds (n = 15) and ionic interactions (n = 3). TGF-β:Ndk exhibits a smaller number of hydrophobic interactions (n = 2), but it compensates with a higher number of main chain-side chain hydrogen bonds (n = 9) and side chain-side chain hydrogen bonds (n = 5). TGF-β:PV shows a balanced distribution of hydrophobic interactions (n = 4), main chain-side chain hydrogen bonds (n = 9), and side chain-side chain hydrogen bonds (n = 10).

Moving on to the NF-κB complexes, NF-κB:FKBP12 displays a moderate number of main chain-side chain hydrogen bonds (n = 13) and side chain-side chain hydrogen bonds (n = 10). NF-κB:Ndk demonstrates similar trends with a slightly higher count of main chain-side chain hydrogen bonds (n = 11). NF-κB:PV has fewer interactions overall, with noticeable contributions from ionic interactions (n = 15) and main chain-side chain hydrogen bonds (n = 5). These results highlight the diverse nature of intermolecular interactions in the studied complexes. Hydrophobic interactions play a crucial role in stabilizing the TGF-β:FKBP12 complex, while main chain-side chain and side chain-side chain hydrogen bonds contribute significantly to the stability of TGF-β:Ndk and TGF-β:PV complexes [45–47]. The NF-κB complexes also exhibit a variety of interactions, with main chain-side chain hydrogen bonds and side chain-side chain hydrogen bonds playing prominent roles.

3.2.3. Molecular dynamics (MD) simulation

The MD simulation results provided detailed insights into the behavior of the protein-protein complexes formed between both TGF-β and NF-κB and its interacting proteins. For TGF-β complexes, the average Root Mean Square Deviation (RMSD) values ranged from 2.274 to 2.514 Å, indicating that TGF-β maintained a relatively stable conformation throughout the 100 ns simulation without any significant spikes, except in the TGF-β:Ndk complex (Fig. 6a). To assess the flexibility profile of individual amino acid residues of TGF-β, the root mean square fluctuation (RMSF) was calculated based on the protein dynamics observed during the MD simulation. The average RMSF values ranged from 0.974 to 0.982 Å, suggesting moderate flexibility in different protein regions. The RMSF analysis provides insights into the mobility and flexibility of specific residues within the protein structure, which can indicate their functional roles [48,49]. In the case of the Ndk and parvalbumin complexes with TGF-β, it was observed that these complexes disrupted hydrogen bonds with specific residues, namely Gly 188, Ser 189, Arg 215, Phe 216, Ser 387, Ile 388, Asn 389, Met 390, Lys 391, His 392, Pro 433, and Ser 434 (Fig. 6b).

This disruption of hydrogen bonds resulted in a higher fluctuation of these residues compared to the FKBP12 complex and the apo-protein of TGF-β. This higher fluctuation suggests increased mobility and flexibility of these residues when Ndk and parvalbumin are bound to TGF-β. The higher flexibility observed in these specific residues indicates that Ndk and parvalbumin from Striatin have the potential to act as inhibitors, similar to the standard inhibitor FKBP12. The disruption of hydrogen bonds and increased flexibility in these residues suggests that Ndk and parvalbumin can potentially interfere with the functional interactions of TGF-β, thereby modulating its signaling pathways. The similarity in flexibility patterns between Ndk, parvalbumin, and FKBP12 further supports their potential inhibitory roles. These findings highlight the importance of specific residues in the interaction between TGF-β and its binding partners and the potential of Ndk and parvalbumin from Striatin to disrupt these interactions and act as inhibitors.

The Radius of Gyration (RoG) analysis showed average values ranging from 1.585 to 1.868 nm, indicating a compact overall shape

Table 3
Docking score, estimated free energy of binding (ΔG), estimated binding affinity (*Kd*) in 37 °C, and energy parameters of the protein-protein complexes.

Parameter	TGF-β:FKBP12	TGF-β:Ndk	TGF-β:PV	NF-κB:FKBP12	NF-κB:Ndk	NF-κB:PV
HADDOCK score	−158.0 ± 2.1	−91.4 ± 9.5	−83.3 ± 2.0	−102.3 ± 7.6	−102.3 ± 7.1	−100.0 ± 3.0
Binding affinity ΔG (kcal/mol)	−11.1	−10.1	−10.3	−11.1	−11.0	−9.4
Kd (M)	$1.4e^{-08}$	$8.0e^{-08}$	$5.1e^{-08}$	$1.4e^{-08}$	$1.5e^{-08}$	$2.3e^{-07}$
Cluster size	200	75	149	90	70	120
RMSD	0.5 ± 0.3	1.6 ± 0.2	1.1 ± 0.3	1.8 ± 0.1	0.8 ± 0.5	1.3 ± 0.1
Van der Waals energy	−85.9 ± 0.9	−50.0 ± 4.2	−41.4 ± 2.9	−47.0 ± 9.1	−53.8 ± 3.8	−24.2 ± 3.8
Electrostatic energy	−253.4 ± 9.0	−184.4 ± 35.8	−188.2 ± 17.6	−399.8 ± 32.9	−321.0 ± 61	−502.4 ± 23.3
Desolvation energy	−22.6 ± 0.8	−6.8 ± 1.3	−12.0 ± 2.2	15.1 ± 4.4	14.2 ± 6.5	20.7 ± 2.9
Restraints violation energy	12.7 ± 4.5	22.8 ± 8.5	77.3 ± 15.7	95.1 ± 10.9	14.4 ± 15.6	40.3 ± 38.7
Buried surface area	2167.1 ± 15.9	1589.5 ± 143.7	1404.3 ± 60.4	1981.2 ± 122.3	1938.0 ± 87.5	1451.6 ± 21.2
Z-score	0.0	−1.3	−1.4	−0.9	−1.8	−1.3

Table 4
Intermolecular interactions in the protein-protein complexes.

Complex	Hydrophobic Interactions	Main Chain-Main Chain Hydrogen Bonds	Main Chain-Side Chain Hydrogen Bonds	Side Chain-Side Chain Hydrogen Bonds	Ionic Interactions	Cation-Pi Interactions
TGF-β complexes						
TGF-β: FKBP12	15	2	6	15	3	1
TGF-β:Ndk	2	0	9	5	5	4
TGF-β:PV	4	1	9	10	4	1
NF-κB complexes						
NF-κB: FKBP12	3	0	13	10	5	2
NF-κB:Ndk	2	1	11	11	8	1
NF-κB:PV	0	1	5	8	15	0

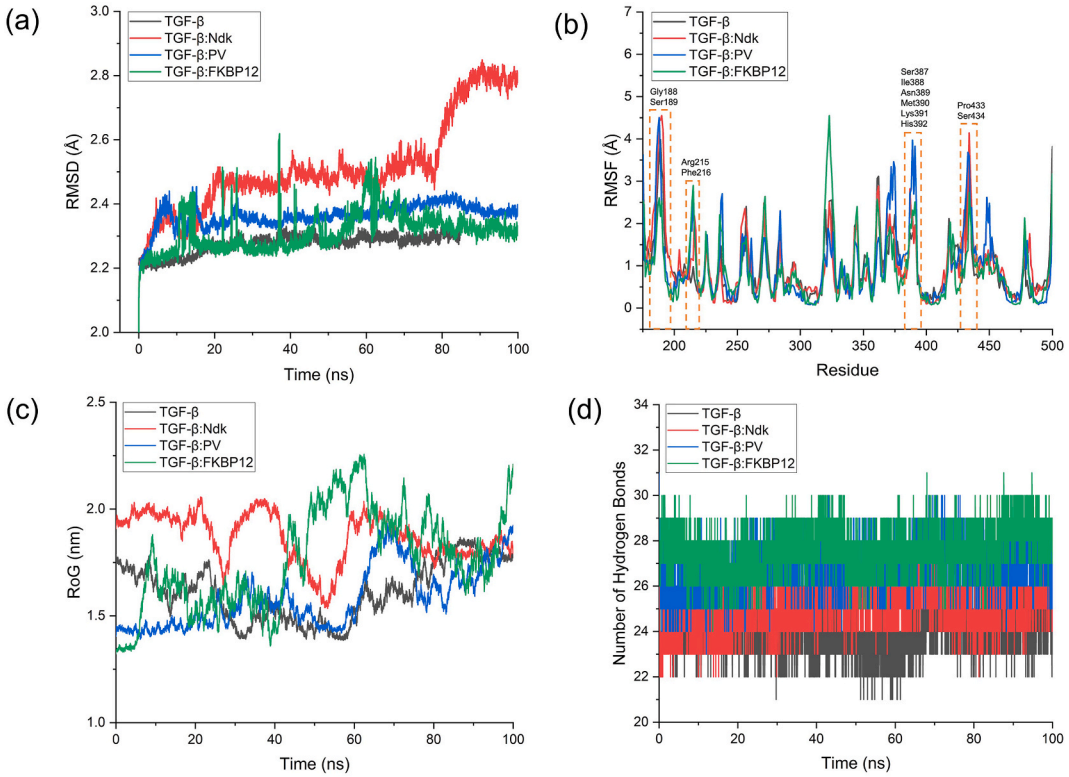

Fig. 6. Molecular dynamics (MD) simulation analysis of TGF-β complexes. (a) Root mean square deviation (RMSD) depicting structural stability, (b) Root mean square fluctuation (RMSF) illustrating residue flexibility, (c) Radius of gyration (RoG) indicating structural compactness, and (d) Number of hydrogen bonds highlighting intermolecular interactions.

for the TGF-β complexes (Fig. 6c). These results demonstrate the stability and structural integrity of the TGF-β complexes during the simulation [50]. The potential energy values reflect the energetics of the protein complexes. All TGF-β complexes exhibited negative potential energies, with values ranging from −321,890.52 to −520,287.71 kcal/mol. These negative values indicate that the formation of the protein-protein complexes is energetically favorable and thermodynamically stable [51,52]. The number of hydrogen bonds formed within two interacting proteins in the TGF-β complexes varied, with values ranging from 24 to 28 (Fig. 6d). The presence of a significant number of hydrogen bonds indicates the existence of strong intermolecular interactions between TGF-β and its interacting proteins, contributing to the stability and specificity of the complexes [53]. The details about Time-averaged structural properties obtained from the MD simulations of TGF-β and NF-κB protein-protein complexes can be seen in Table 4.

Regarding the NF-κB complexes, the average RMSD values ranged from 2.469 to 2.753 Å without any notable spikes (Fig. 7a), suggesting relatively stable conformations during the MD simulation. The average RMSF values ranged from 0.863 to 1.127 Å, indicating moderate flexibility in different regions of the NF-κB complexes. In the case of the Ndk complex with NF-κB, it was observed that the complex disrupted hydrogen bonds with specific residues, namely Gly 64, Pro 65, Ser 66, His 67, Thr146, Lys 147, and Lys 148 (Fig. 7b). This disruption of hydrogen bonds resulted in a higher fluctuation of these residues compared to the FKBP12 complex and the apo-protein of NF-κB. This higher fluctuation suggests increased mobility and flexibility of these residues when Ndk is bound to NF-κB. Furthermore, it was found that both the Ndk and parvalbumin complexes exhibited similar fluctuation patterns as the FKBP12 complex in certain residues, specifically residue numbers 263, 264, 265, 278, and 279. This similarity in flexibility patterns suggests that Ndk and parvalbumin from Striatin have the potential to act as inhibitors, similar to the standard inhibitor FKBP12. The higher flexibility observed in these specific residues indicates their potential importance in modulating the functional interactions of NF-κB. These findings indicate that Ndk and parvalbumin have the potential to disrupt the interactions of NF-κB with specific residues, potentially interfering with its signaling pathways. The similarity in flexibility patterns with the standard inhibitor FKBP12 further supports their potential inhibitory roles. However, further experimental studies are needed to validate the inhibitory effects of Ndk and parvalbumin on NF-κB signaling and to elucidate the underlying mechanisms of their interactions with NF-κB and their functional implications.

The RoG analysis showed average values ranging from 2.048 to 2.213 nm, indicating a compact overall shape for the NF-κB complexes (Fig. 7c). These results suggest that NF-κB maintained stable structures with moderate flexibility throughout the simulation. Similar to the TGF-β complexes, the NF-κB complexes exhibited negative potential energies, ranging from −496,164.16 to −516,520.93 kcal/mol (Table 5). These negative values indicate favorable and stable binding interactions between NF-κB and its interacting proteins. The number of hydrogen bonds formed within the NF-κB complexes varied, with values ranging from 20 to 29 (Fig. 7d). The presence of significant hydrogen bonding interactions suggests strong intermolecular interactions, contributing to the

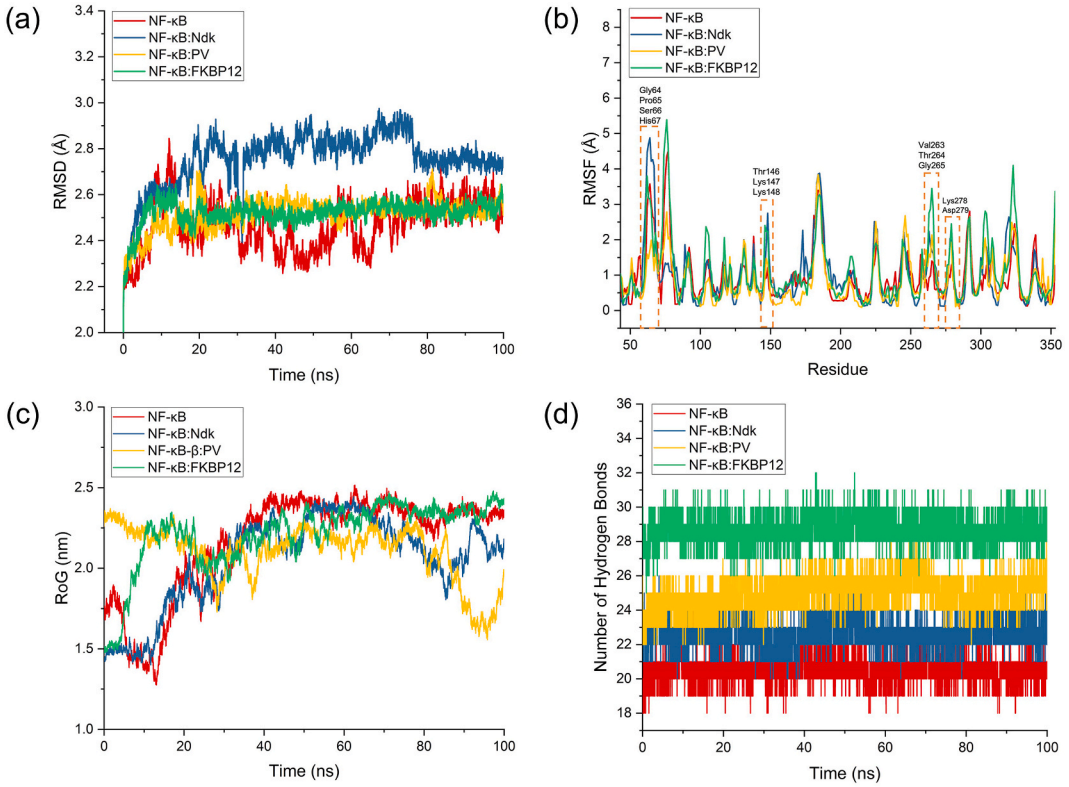

Fig. 7. Molecular Dynamics (MD) simulation results for NF-κB complexes, illustrating the dynamics and stability of the protein-protein interactions. (a) Root Mean Square Deviation (RMSD), (b) Root Mean Square Fluctuation (RMSF), (c) Radius of Gyration (RoG), and (d) Number of hydrogen bonds.

Table 5
Time-averaged structural properties obtained from the MD simulations of TGF-β and NF-κB protein-protein complexes.

Complex	Average RMSD (Å)	Average RMSF (Å)	Average RoG (nm)	Potential energy (kcal/mol)	Number of hydrogen bonds between the two proteins
TGF-β complexes					
TGF-β	2.274	0.974	1.612	−250,706.52	24
TGF-β:FKBP12	2.310	0.895	1.763	−520,287.71	28
TGF-β:Ndk	2.513	0.990	1.868	−356,330.76	25
TGF-β:PV	2.364	0.982	1.585	−321,890.52	27
NF-κB complexes					
NF-κB	2.469	0.979	2.162	−505,702.42	20
NF-κB:FKBP12	2.521	1.127	2.213	−516,520.93	29
NF-κB:Ndk	2.753	1.023	2.048	−509,907.75	23
NF-κB:PV	2.514	0.863	2.101	−496,164.16	25

stability and specificity of the NF-κB complexes.

3.2.4. MM/PBSA binding free energy calculations

These MM/PBSA calculations provide valuable insights into the protein-protein complexes' thermodynamic stability and binding affinities (Table 6). These values were important in supporting the findings obtained from previous analyses. The $\Delta G_{binding}$ values represent the binding free energy of each complex, with the mean value indicated along with the corresponding standard deviation in units of kcal/mol. Similar to the results of protein-protein docking, the TGF-β:FKBP12 complex exhibits the highest negative $\Delta G_{binding}$ value, indicating a strong binding affinity between TGF-β and FKBP12. The TGF-β:Ndk and TGF-β:PV complexes showed relatively lower negative $\Delta G_{binding}$ values, suggesting weaker binding compared to the TGF-β:FKBP12 complex. While, the NF-κB:FKBP12 complex displays a negative $\Delta G_{binding}$ value, indicating favorable binding affinity. The NF-κB:Ndk and NF-κB:PV complexes also exhibited negative $\Delta G_{binding}$ values, albeit lower than that of NF-κB:FKBP12. The results indicate that the TGF-β:FKBP12 complex has

Table 6
Result of the MM/PBSA calculations for the protein−protein complexes. The mean $\Delta G_{binding}$ is shown with standard deviation in units of kcal/mol.

Complex	MM/PBSA Calculation Results $\Delta G_{binding}$ (kcal/mol)			Average (kcal/mol)
	I	II	III	
TGF-β complexes				
TGF-β:FKBP12	−89.66 ± 5.6	−90.58 ± 5.5	−90.12 ± 5.7	−90.12
TGF-β:Ndk	−38.93 ± 7.3	−38.61 ± 6.1	−39.27 ± 7.6	−38.94
TGF-β:PV	−37.35 ± 7.6	−37.27 ± 7.8	−37.34 ± 7.1	−37.32
NF-κB complexes				
NF-κB:FKBP12	−51.71 ± 6.4	−51.66 ± 6.7	−51.77 ± 5.2	−51.71
NF-κB:Ndk	−35.87 ± 6.4	−35.95 ± 5.5	−35.92 ± 5.2	−35.91
NF-κB:PV	−36.19 ± 7.2	−35.03 ± 6.7	−34.67 ± 6.0	−35.30

the strongest binding affinity among all the complexes studied, as evidenced by the most negative average $\Delta G_{binding}$ value. The NF-κB complexes, particularly NF-κB:Ndk and NF-κB:PV, also show favorable binding affinities but to a lesser extent compared to the TGF-β complexes.

Fig. 8 illustrates a comprehensive view of the binding free energy landscape concerning individual amino acids within the context of the Ndk and PV complexes. This plot provides valuable insights into the specific amino acid residues that contribute significantly to the binding interactions between Ndk and PV and their respective receptors, TGF-β and NF-κB. In the Ndk complexes, the amino acids Asp9, Tyr27, and Ser29, situated within the binding domain, stand out due to their remarkably low binding free energy values of −6.36, −5.52, and −6.45 kcal/mol, respectively. These energy values underscore the strong and stabilizing nature of the interactions formed between these amino acids and the receptors. Such favorable energy values suggest that Asp9, Tyr27, and Ser29 likely contribute residues in establishing a firm and specific binding between Ndk and its receptors (Fig. 8a).

In the context of the PV complexes, the amino acids Lys 21, Phe24, Glu26, and Asp 28, residing within the binding domain, exhibited particularly low binding free energy values of −2.89, −4.76, −6.48, and −2.90 kcal/mol, respectively (Fig. 8b). These energy values were significant in facilitating the robust interaction between PV and its receptors. These findings shed light on the specific amino acids within Ndk and PV that were essential for their binding to TGF-β and NF-κB.

3.3. *In vitro study of striatin*

To complement our *in silico* proteomics studies, we conducted a series of *in vitro* experiments focusing on Striatin. This multifaceted approach aimed to assess Striatin's impact on HepG2 cell viability, investigate its effects on LPS-induced reduction in albumin secretion, and explore its influence on the expression of NF-κB. These *in vitro* studies provide preliminary insights into Striatin's effects on HepG2 cell viability, LPS-induced reduction in albumin secretion, and modulation of NF-κB expression. While these findings are promising, they should be viewed as part of an ongoing investigation into Striatin's therapeutic potential.

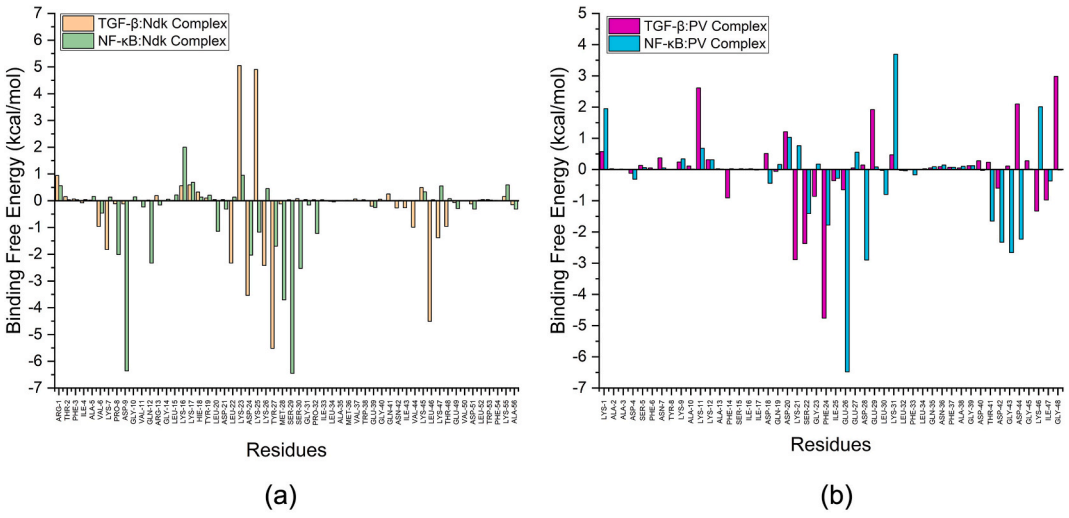

Fig. 8. Plot illustrating the binding free energy landscape of individual amino acids within Ndk and PV complexes. (a) Binding free energy plot for Ndk complexes. (b) Binding free energy plot for PV complexes.

3.3.1. Effect of Striatin on the viability of HepG2 cells

The viability assay of Striatin on HepG2 cells is shown in Fig. 9. Based on this figure, Striatin at a concentration of 5–40 μg/mL did not decrease the HepG2 cell number, indicating safety.

3.3.2. Determination of optimal LPS concentration to suppress albumin gene expression and extracellular secretion in HEPG2 cells

The albumin gene expression and extracellular albumin secretion were analyzed in response to LPS treatment. As shown in Fig. 10a, LPS concentration influenced the suppression of albumin synthesis. However, while a slight trend was observed, the changes in albumin mRNA expression were not statistically significant. Similarly, extracellular albumin secretion (Fig. 10b) showed a general trend in line with mRNA expression, although the correlation between the two was not robust or statistically significant. Fig. 10c indicates that the highest suppression of albumin gene expression occurred after 24 h (47.1 %). Over prolonged incubation, the suppression effect decreased, with the lowest extracellular albumin content recorded at 24 h (77.4 %) (Fig. 10d).

3.3.3. Striatin effect on LPS-induced hypoalbumin

In setting the concentration gradient, we utilized a range of concentrations spanning from 0 μg/ml to a maximum of 40 μg/ml of Striatin. This range was chosen based on preliminary viability assays conducted on HEPG2 cells, as depicted in Fig. 9 of our manuscript. The results of this assay demonstrated that even at the highest concentration tested (40 μg/ml), Striatin did not significantly reduce HEPG2 cell viability compared to untreated cells (0 μg/ml). Therefore, this concentration gradient allowed us to explore a range of doses while ensuring cell viability remained unaffected.

As seen in Fig. 11a, 20 μg/mL of Striatin showed the optimal stimulatory effect on albumin gene expression. Higher Striatin concentrations, unfortunately, did not further enhance the albumin expression. Striatin treatment positively affected albumin expression when co-incubated with the substance-suppressing albumin, LPS. As can be seen in Fig. 11b, the detection of extracellular albumin secreted by the cell treated with 20 μg/mL of Striatin indicated the most effective concentration of Striatin. The addition of 10 μg/mL of HSA produced lower albumin extracellular content than the untreated group.

As shown in Fig. 11c, the most effective incubation time is 24 h. Prolonged incubation even decreased the effect of Striatin. Furthermore, the results show the albumin extracellular secretion increment and culture time, indicating continuous albumin synthesis by the cells (Fig. 11d). LPS had a short-term effect on reducing HSA production. Treatment with Striatin normalized cell function due to LPS exposure, and this effect lasted until the end of observation (72 h).

3.3.4. Striatin effect on NF-κB expression

The expression of NF-κB, a key signaling molecule of the inflammatory response, was investigated to observe the effect of Striatin on the inflammation pathway. LPS significantly increased NF-κB expression after 24 h of incubation. Co-incubation of Striatin and LPS significantly reduced NF-κB expression. The addition of 20 μg/mL of Striatin had the highest effect on NF-κB inhibition during co-incubation treatment.

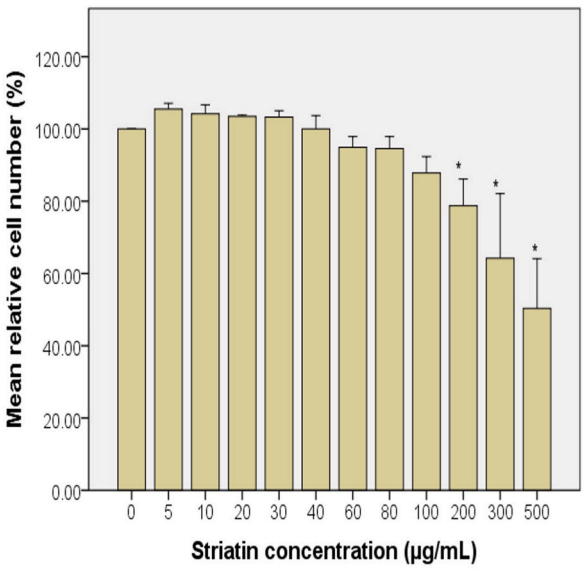

Fig. 9. Effect of varying concentrations of Striatin extract on HepG2 cell viability. Data are represented as mean ± standard deviation. Statistical significance indicated by * ($p < 0.05$) compared to the control group (0 μg/mL Striatin).

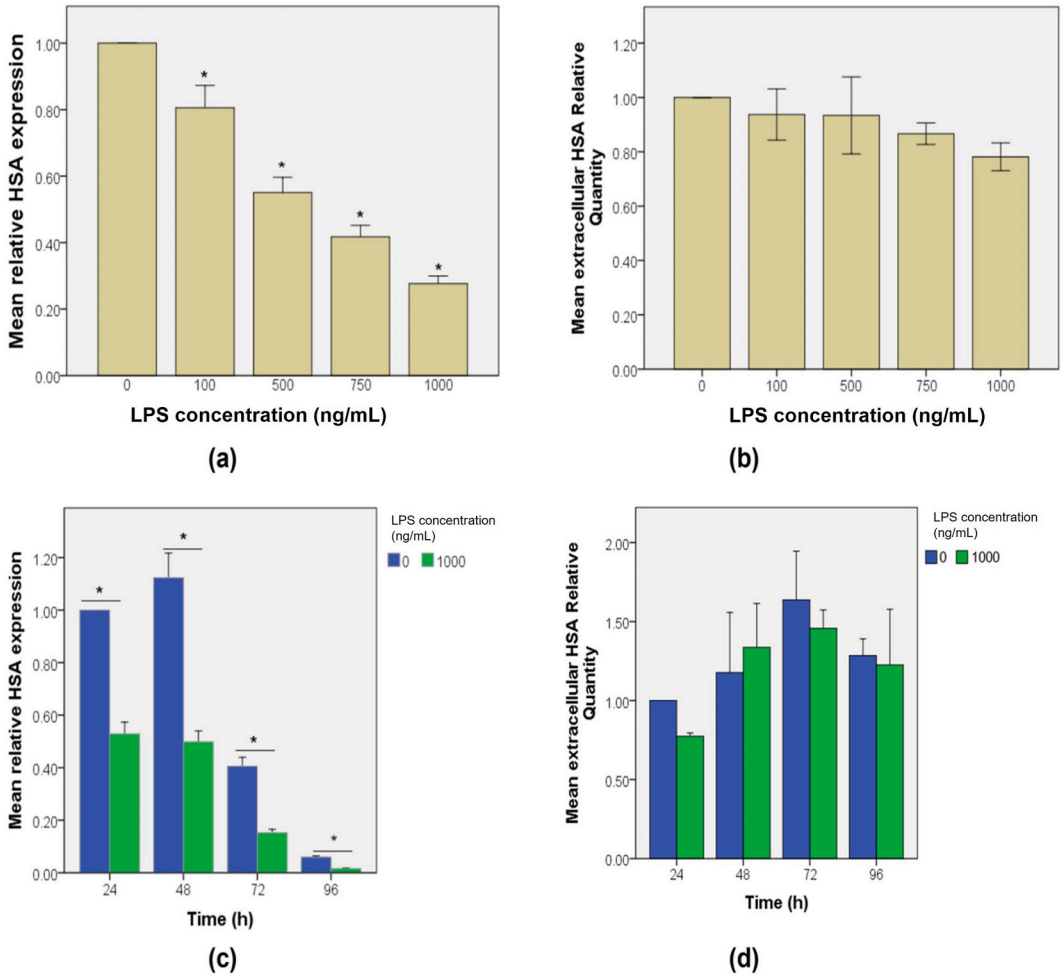

Fig. 10. Optimal Lipopolysaccharide (LPS) treatment conditions for the suppression of (a) albumin mRNA expression and (b) extracellular albumin secretion in HepG2 cells. Time course analysis of LPS treatment illustrating the induction of suppression in (c) albumin mRNA expression and (d) extracellular albumin secretion. *$p < 0.05$, indicating statistical significance.

4. Discussion

The proteomics analysis conducted in this study provided valuable insights into the protein composition of Striatin. The presence of Ndk and PV in Striatin was confirmed by analyzing protein bands and subsequent identification using LC-MS/MS. These findings are consistent with previous studies on Striatin and other related complexes. Several studies have reported the presence of Ndk in various biological systems and highlighted its diverse functions. For instance, Ndk has been implicated in nucleotide metabolism, phosphorylation-dependent signaling pathways, and regulation of cellular processes such as DNA repair and apoptosis [54,55]. Similarly, PV, a calcium-binding protein, has been shown to play a role in calcium homeostasis, muscle contraction, and signal transduction [56,57]. The identification of Ndk and PV in Striatin aligns with their known functions and suggests their potential involvement in the biological processes associated with this complex.

The *in silico* investigations aimed to unravel the protein-protein interactions and binding characteristics of Striatin components with TGF-β and NF-κB. The results obtained from the 3D modeling, protein-protein docking simulations, MD simulations, and binding free energy calculations shed light on these interactions' structural and dynamic aspects. Using computational methods, the 3D model construction of Ndk and PV allowed for a detailed examination of their active sites and potential interaction interfaces. The identification of specific amino acid residues within the active sites of Ndk and PV provides crucial insights into the key molecular interactions that contribute to their binding with TGF-β and NF-κB. The protein-protein docking simulations revealed the binding modes and affinities of the complexes formed between FKBP12 (as the standard inhibitor), Ndk, and PV with TGF-β, and NF-κB (as the target receptors). The results showed that the TGF-β:FKBP12 complex exhibited the strongest binding affinity, consistent with previous studies [58,59]. FKBP12, a well-known inhibitor, has been extensively studied for its ability to regulate TGF-β signaling by interfering with the binding of TGF-β to its receptors [60,61]. The favorable binding affinity observed between TGF-β and FKBP12 in our study reinforces the notion that FKBP12 can effectively inhibit TGF-β-mediated signaling.

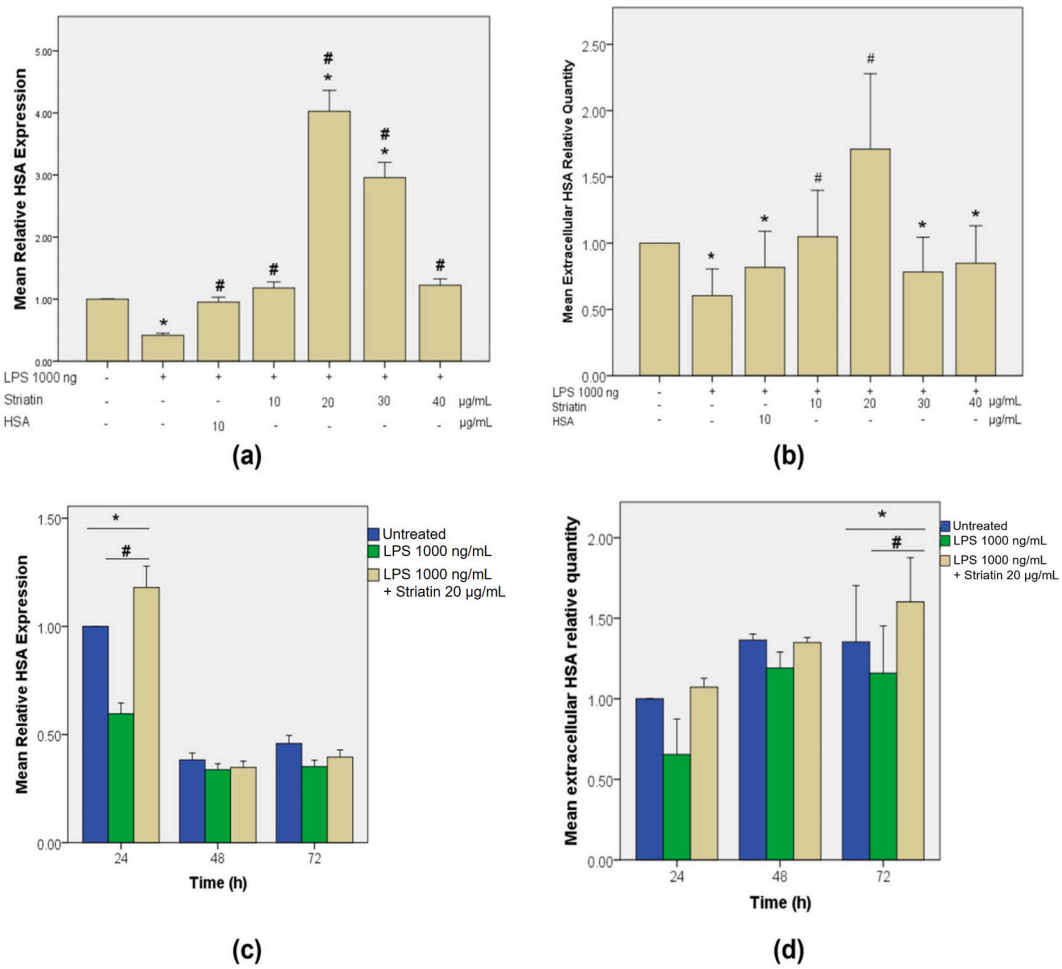

Fig. 11. Optimal Striatin concentration to recover (a) albumin gene expression suppression and (b) albumin extracellular suppression. Time course Striatin treatment to recover (c) albumin gene expression suppression and (d) albumin extracellular suppression in HEPG2 cells. *p < 0.05 vs. untreated group (0 ng/mL LPS); #p < 0.05 vs. LPS alone group (1000 ng/mL LPS).

Interestingly, both Ndk and PV complexes exhibited hydrogen bond formation with specific residues of TGF-β and NF-κB, similar to FKBP12. Hydrogen bonds play a critical role in stabilizing protein-protein interactions and can contribute to the strength and specificity of binding [62,63]. The formation of hydrogen bonds between Ndk, PV, and the target receptors suggests their potential inhibitory effects by adopting binding poses that resemble FKBP12. These findings are supported by previous studies demonstrating the inhibitory role of Ndk and PV in different biological contexts [64,65]. The disruption of hydrogen bonds and increased flexibility in specific residues observed in the MD simulations further support the potential of Ndk and PV as inhibitors of TGF-β and NF-κB signaling.

The MD simulations provided insights into the stability and flexibility of the protein-protein complexes formed between FKBP12, Ndk, and PV with TGF-β, and NF-κB. The RMSD analysis indicated relatively stable conformations for both TGF-β and NF-κB complexes, supporting the robustness of the interactions observed in the docking simulations. The RMSF analysis revealed moderate flexibility in different regions of the complexes, suggesting inherent dynamics within the protein-protein interfaces. Importantly, the disruption of hydrogen bonds and increased flexibility observed in specific residues of Ndk and PV complexes highlight their potential inhibitory effects. These findings are in line with previous studies reporting the importance of specific residues and their flexibility in modulating protein-protein interactions and signaling pathways [66,67]. The similarity in flexibility patterns between Ndk, PV, and FKBP12 further supports their potential inhibitory roles. Notably, our findings are consistent with the inhibitory effects of Ndk and PV observed in other systems [68,69]. The disruption of interactions and increased flexibility of specific residues suggest that Ndk and PV have the potential to interfere with the functional interactions of TGF-β and NF-κB, thereby modulating their signaling pathways.

The binding free energy calculations using the MM/PBSA approach further support the findings obtained from the docking simulations and MD simulations. The negative values of $\Delta G_{binding}$ indicate favorable binding affinities for the TGF-β and NF-κB complexes. The TGF-β:FKBP12 complex exhibited the strongest binding affinity among all the complexes studied, consistent with the lower docking scores and higher free energy of binding. This reaffirms the potent inhibitory role of FKBP12 in TGF-β signaling and its

potential as a therapeutic target [70,71]. The NF-κB complexes, particularly NF-κB:Ndk and NF-κB:PV, also showed favorable binding affinities, albeit to a lesser extent compared to TGF-β complexes.

The results obtained in this study align with previous findings from other research groups investigating the interactions of TGF-β and NF-κB with their binding partners. For instance, studies have reported the inhibitory effects of FKBP12 on TGF-β signaling by disrupting the TGF-β-receptor interactions [40,72]. Our findings support these observations and further suggest that Ndk and PV, with their similar flexibility patterns and hydrogen bond formations, can potentially exert similar inhibitory effects on TGF-β signaling. Similarly, investigations into the regulatory mechanisms of NF-κB signaling have identified various proteins and factors that modulate its activity. Previous studies have reported the inhibitory effects of Ndk and PV on NF-κB signaling through distinct mechanisms [73–75]. The present study complements these findings by providing detailed structural insights into the interactions between Ndk, PV, and NF-κB, further supporting their potential inhibitory roles.

The consistency between our findings and previous studies underscores the robustness and reliability of the *in silico* methods employed in this research. Furthermore, the integration of proteomics analysis with *in silico* approaches provides a comprehensive understanding of the protein composition, interactions, and potential inhibitory effects of Striatin components. This holistic approach contributes to our knowledge of the complex molecular mechanisms underlying Striatin-mediated cellular processes and highlights the potential therapeutic implications of Ndk and PV as inhibitors in TGF-β and NF-κB signaling pathways.

To enhance and validate the findings from our *in silico* proteomics studies, we undertook a comprehensive series of *in vitro* experiments specifically centered around the bioactive protein fraction from *Channa striata* known as Striatin. These *in vitro* investigations were designed to bridge the gap between computational predictions and practical applications, allowing us to understand better how Striatin functions at the cellular level. By conducting these experiments, we aimed to provide tangible evidence and insights into Striatin's impact on critical cellular processes, including albumin synthesis and the regulation of inflammatory responses, ultimately contributing to a more holistic comprehension of its therapeutic potential. This study investigated the effect of LPS on albumin synthesis at both gene and protein levels, measured with qPCR and sandwich ELISA, respectively. Based on the assays, 1000 ng of LPS suppressed the albumin expression and secretion in HepG2 cells. *Channa striata* (snakehead fish) has been widely known for its therapeutic applications. One of its notable activities is albumin stimulation under infection or wounded conditions. Consumption of snakehead fish extract for post-operative patients significantly increases their serum albumin levels compared with pre-treatment conditions [76].

The HepG2 cells could secrete protein through cholesterol metabolism and amino acid pathways [6]. Few amino acids have been known to exert an anti-inflammatory effect by regulating the NF-κB signaling pathway in the intestinal cells [77]. The NF-κB was used in this study as an inflammatory parameter since it is the transcription factor key that initiates the acute phase response of hepatic cells [78]. In this study, the specific protein type of NF-κB that was examined is the nuclear factor kappa B subunit 1 (NF-κB1). NF-κB1 is a crucial component of the NF-κB transcription factor family, which plays a central role in regulating genes involved in immune responses, inflammation, cell survival, and proliferation [79,80]. NF-κB1 is involved in the classical NF-κB signaling pathway and is implicated in various cellular processes, including the inflammatory response [81]. In this context, the study focused on investigating the effect of Striatin on the expression of NF-κB1 in HepG2 cells exposed to lipopolysaccharide (LPS)-induced inflammation. The decision to focus solely on NF-κB expression in the *in vitro* experiments was based on several factors. Firstly, during preliminary assays, we observed inconsistent results regarding TGF-β gene expression when induced by LPS in HEPG2 cells. Increasing LPS concentrations appeared to reduce TGF-β gene expression, but the results were not conclusive. Secondly, our molecular dynamics (MD) simulations

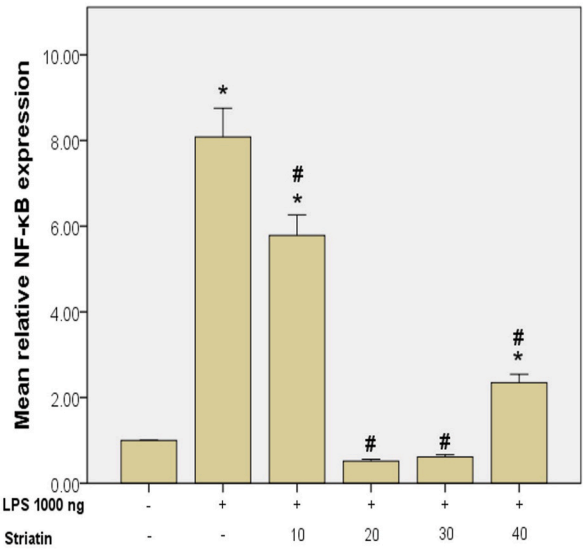

Fig. 12. Effect of Striatin treatment on NF-κB expression in HepG2 cells under LPS-induced inflammation. *p < 0.05 compared to the untreated group (0 ng/mL LPS); #p < 0.05 compared to the LPS alone group (1000 ng/mL LPS), indicating significant differences.

indicated that the proteins from Striatin exhibited interactions more comparable to a standard antagonist when interacting with NF-κB rather than with TGF-β. This suggested a potentially stronger inhibitory effect on the NF-κB expression. Given these factors and the primary focus of our study on albumin expression, we made the decision not to pursue further analysis of TGF-β expression *in vitro*. Instead, we chose to concentrate our efforts on investigating the effect of Striatin on NF-κB expression, which aligned more closely with the objectives of our research.

High expression of NF-κB in LPS control (Fig. 12) indicated the relationship between albumin suppression along NF-κB activation during an inflammatory response, which has also been investigated in rat hepatocytes [9]. Striatin has been shown to suppress NF-κB expression, in line with its effect in increasing albumin expression. Striatin increases albumin expression and secretion in LPS-induced HepG2 cells as a recovery process due to its anti-inflammatory effect. However, it is also reported that HSA can bind to LPS and other bacterial products (e.g., lipoteichoic acid and peptidoglycan) [82]. This study found that the effect of Striatin to recover albumin expression and secretion was through interfering with NF-κB expression. Snakehead fish extract has also been studied for its anti-inflammatory activities. Snakehead fish extract consumption after cesarean section also normalizes blood leukocyte numbers compared to control [83]. Its consumption in pulmonary tuberculosis patients significantly reduces inflammatory cytokines levels [84]. These findings raise the promise of Striatin in patients with inflammation-related hypoalbuminemia conditions.

5. Comparison with similar studies, novelty, and significance of the study

Several studies have investigated the effects of bioactive compounds on NF-κB expression and inflammatory pathways. For instance, a study by Wang et al. (2006) examined the anti-inflammatory effects of a novel peptide on NF-κB p50 subunit signaling in human hepatocytes, demonstrating a significant reduction in NF-κB activity. This peptide effectively interacted with the NF-κB p50 subunit. It inhibited the production of TNF-α and IL-6 in the THP-1 cell line, PMA-induced ear edema, and zymosan A-induced peritonitis in mice [85]. Similarly, Chakrabarti et al. (2014) explored the therapeutic potential of marine-derived bioactive peptides on chronic inflammation, reporting notable decreases in pro-inflammatory cytokine levels and NF-κB activity *in vitro* [86]. Unlike previous studies, we utilized a combination of *in silico proteomics* and *in vitro* approaches to elucidate the molecular interactions and mechanisms underlying Striatin's anti-inflammatory effects. The novelty and significance of this study lie in its multifaceted approach towards unraveling the therapeutic potential of Striatin, a bioactive protein fraction derived from *Channa striata*. By integrating *in silico* proteomics analyses with *in vitro* experiments, the research endeavored to comprehensively decipher the molecular mechanisms and therapeutic implications of Striatin. Through proteomics analysis, two novel proteins, nucleoside diphosphate kinase (Ndk) and parvalbumin (PV), were identified and characterized within Striatin, representing a significant step forward in understanding its molecular composition. These proteins, previously unexplored in the context of hypoalbuminemia, offered new avenues for investigation. Utilizing advanced computational techniques such as molecular modeling, protein-protein docking, and molecular dynamics simulations, the study elucidated the molecular interactions between Ndk, PV, and their target receptors, including TGF-β and NF-κB. This detailed analysis provided insights into the structural dynamics and binding affinities underlying the inhibitory effects of Striatin on key cellular expression associated with hypoalbuminemia and inflammation. The computational predictions were further validated through *in vitro* experiments, which confirmed the therapeutic effects of Striatin, particularly its ability to modulate NF-κB expression and restore albumin levels in LPS-induced HepG2 cells. The findings of the study not only corroborated the computational predictions but also provided tangible evidence of Striatin's potential as an intervention for inflammation-related hypoalbuminemia. By elucidating the molecular mechanisms through which Striatin exerts its therapeutic effects, the research laid the groundwork for future clinical investigations. Striatin, with its unique protein composition and inhibitory properties, emerged as a promising candidate for drug development and personalized medicine approaches targeting conditions characterized by hypoalbuminemia and inflammation.

6. Limitations and future works

While this study provided valuable insights into the therapeutic potential of Striatin, several limitations warrant consideration for future research endeavors. Firstly, the *in vitro* experiments focused primarily on the effect of Striatin on NF-κB expression and albumin synthesis in HepG2 cells. While these findings shed light on the molecular mechanisms underlying Striatin's therapeutic effects, further investigations are needed to comprehensively elucidate its broader impact on other signaling pathways and cellular processes implicated in hypoalbuminemia and inflammation. Therefore, it will be important to explore the effects of Striatin on additional key signaling molecules involved in the inflammatory response, such as interleukin-6 (IL-6) and tumor necrosis factor-alpha (TNF-α). This expansion aims to provide a more comprehensive understanding of Striatin's anti-inflammatory properties and its potential therapeutic applications. Additionally, the computational modeling approaches employed in this study relied on protein sequences and structural templates available in existing databases. Despite their utility, these methods are subject to inherent limitations, such as inaccuracies in template selection and modeling assumptions. Future research could benefit from advanced computational techniques, and structural biology approaches to refine and validate the predicted molecular interactions and binding affinities of Striatin components with their target receptors. Furthermore, the *in vitro* experiments focused primarily on cellular models, which may not fully capture the complex physiological and pathological processes observed *in vivo*. Future studies could explore the therapeutic efficacy of Striatin in animal models of hypoalbuminemia and inflammation to validate the findings obtained from cell culture experiments and to assess its safety profile and pharmacokinetics. Moreover, while the present study identified Ndk and PV as potential therapeutic targets within Striatin, their precise mechanisms of action and downstream effects on cellular pathways remain to be fully elucidated. Future research could delve deeper into the functional roles of Ndk and PV in modulating TGF-β and NF-κB signaling pathways and explore their interactions with other cellular components.

7. Conclusion

In conclusion, this study employed a dual approach, combining *in silico* proteomics and *in vitro* methods, to investigate Striatin's protein composition, molecular interactions, and potential bioactivity. Notably, our findings confirm Ndk and PV in Striatin, implying their involvement in its complex mechanisms. The *in silico* analysis highlighted that Ndk and PV could modulate TGF-β and NF-κB signaling pathways through inhibitory effects, supported by the disruption of hydrogen bonds and increased flexibility in specific residues. As a confirmation of the *in silico* studies, *in vitro* experiments demonstrated that Striatin possesses the capacity to suppress NF-κB expression and normalize albumin levels in HepG2 cells exposed to LPS-induced reduction in albumin secretion. These results underscore Striatin's potential as an intervention for inflammation-related hypoalbuminemia. Further research, including *in vivo* studies, holds promise for exploring Striatin's therapeutic potential.

Funding

This research is under PT Dexa Medica's concern and support, including publication fees.

Disclosure statement

The authors confirm that no AI tools were used in the preparation or writing of this manuscript. All data analysis, manuscript preparation, and writing were performed manually by the authors without the assistance of artificial intelligence tools.

Ethics declarations

Review and/or approval by an ethics committee was not needed for this study because the *in silico* proteomics analyses and subsequent *in vitro* experiments conducted on Striatin did not involve direct human or animal subjects.

Data availability statement

Data will be made available on request.

CRediT authorship contribution statement

Affina Musliha: Writing – original draft, Visualization, Validation, Methodology, Data curation, Conceptualization. **Doni Dermawan:** Writing – original draft, Visualization, Validation, Methodology, Formal analysis, Data curation, Conceptualization. **Puji Rahayu:** Writing – review & editing, Supervision, Methodology, Formal analysis, Conceptualization. **Raymond R. Tjandrawinata:** Writing – review & editing, Supervision.

Declaration of competing interest

The authors declare that they have no known competing financial interests or personal relationships that could have appeared to influence the work reported in this paper.

Acknowledgments

The authors acknowledge Prof. Dr. Heni Rachmawati, Prof. Dr. Debbie Soefie Retnoningrum, Destrina Grace Simanjuntak, Ireno Mega Putera Demmangngewa, Novita Herwidayani, and Emilia Utomo for a critical review of this manuscript.

References

[1] V. Gounden, R. Vashisht, I. Jialal, Hypoalbuminemia, StatPearls, StatPearls Publishing LLC., Treasure Island (FL), 2022.
[2] P.B. Soeters, R.R. Wolfe, A. Shenkin, Hypoalbuminemia: pathogenesis and clinical significance, JPEN - J. Parenter. Enter. Nutr. 43 (2019) 181–193.
[3] F.C. Alves, J. Sun, A.R. Qureshi, L. Dai, S. Snaedal, P. Bárány, O. Heimbürger, B. Lindholm, P. Stenvinkel, The higher mortality associated with low serum albumin is dependent on systemic inflammation in end-stage kidney disease, PLoS One 13 (2018) e0190410.
[4] A.S. Almasaudi, R.D. Dolan, C.A. Edwards, D.C. McMillan, Hypoalbuminemia reflects nutritional risk, body composition and systemic inflammation and is independently associated with survival in patients with colorectal cancer, Cancers 12 (2020) 1986.
[5] J.K. Sun, F. Sun, X. Wang, S.T. Yuan, S.Y. Zheng, X.W. Mu, Risk factors and prognosis of hypoalbuminemia in surgical septic patients, PeerJ 3 (2015) e1267.
[6] N. Busso, C. Chesne, F. Delers, F. Morel, A. Guillouzo, Transforming growth-factor-β (TGF-β) inhibits albumin synthesis in normal human hepatocytes and in hepatoma HepG2 cells, Biochem. Biophys. Res. Commun. 171 (1990) 647–654.
[7] R. Sharma, A. Khanna, M. Sharma, V.J. Savin, Transforming growth factor-β1 increases albumin permeability of isolated rat glomeruli via hydroxyl radicals, Kidney Int. 58 (2000) 131–136.
[8] L.M. Russo, W.D. Comper, T.M. Osicka, Mechanism of albuminuria associated with cardiovascular disease and kidney disease, Kidney Int. 66 (2004) S67–S68.
[9] X. Wang, W. Li, J. Lu, N. Li, J. Li, Lipopolysaccharide suppresses albumin expression by activating NF-kappaB in rat hepatocytes, J. Surg. Res. 122 (2004) 274–279.
[10] M. Aminur Rahman, A. Arshad, S.M. Nurul Amin, Growth and production performance of threatened snakehead fish, Channa striatus (Bloch), at different stocking densities in earthen ponds, Aquacult. Res. 43 (2012) 297–302.

[11] A. Jais, Pharmacognosy and pharmacology of Haruan (Channa striatus), a medicinal fish with wound healing properties, Bol. Latinoam. Caribe Plantas Med. Aromat. 6 (2007).
[12] A. Zuraini, M.N. Somchit, M.H. Solihah, Y.M. Goh, A.K. Arifah, M.S. Zakaria, N. Somchit, M.A. Rajion, Z.A. Zakaria, A.M. Mat Jais, Fatty acid and amino acid composition of three local Malaysian Channa spp. fish, Food Chem. 97 (2006) 674–678.
[13] P. Rahayu, F. Marcelline, E. Sulistyaningrum, M. Suhartono, R. Tjandrawinata, Potential effect of Striatin (DLBS0333), a bioactive protein fraction isolated from Channa striata for wound treatment, Asian Pac. J. Trop. Biomed. 6 (2016).
[14] H. Yu, X. Rao, K. Zhang, Nucleoside diphosphate kinase (Ndk): a pleiotropic effector manipulating bacterial virulence and adaptive responses, Microbiol. Res. 205 (2017) 125–134.
[15] L. Zhang, M. Song, N. Yang, X. Zhang, S.H. Abbas Raza, K. Jia, J. Tian, Y. Zhang, D. Zhang, Q. Shi, T. Wu, Y. Kang, G. Hou, A. Qian, G. Wang, X. Shan, Nucleoside Diphosphate Kinases (ndk) reveals a key role in adhesion and virulence of Aeromonas veronii, Microb. Pathog. 149 (2020) 104577.
[16] M.R. Miranda, M. Sayé, C. Reigada, F. Galceran, M. Rengifo, B.J. Maciel, F.A. Digirolamo, C.A. Pereira, Revisiting trypanosomatid nucleoside diphosphate kinases, Mem. Inst. Oswaldo Cruz 116 (2022) e210339.
[17] G. Butera, D. Vecellio Reane, M. Canato, L. Pietrangelo, S. Boncompagni, F. Protasi, R. Rizzuto, C. Reggiani, A. Raffaello, Parvalbumin affects skeletal muscle trophism through modulation of mitochondrial calcium uptake, Cell Rep. 35 (2021) 109087.
[18] E.A. Permyakov, V.N. Uversky, What is parvalbumin for? Biomolecules 12 (2022).
[19] G. Sliwoski, S. Kothiwale, J. Meiler, E.W. Lowe Jr., Computational methods in drug discovery, Pharmacol. Rev. 66 (2014) 334–395.
[20] S. Choudhuri, M. Yendluri, S. Poddar, A. Li, K. Mallick, S. Mallik, B. Ghosh, Recent Advancements in Computational Drug Design Algorithms through Machine Learning and Optimization, Kinases and Phosphatases, 2023, pp. 117–140.
[21] N.A. Taslim, N. Fitriana, N.L.E. Suprapti, C.P. Marsella, A. Bukhari, H. Rasyid, A. Aminuddin, S. As'ad, A.M. Aman, M. Madjid, Effects of Channa striata extract on albumin serum and neutrophil-to-lymphocyte ratio in hyperglycemic rats with wound injury: a randomized control study, Open Access Macedonian Journal of Medical Sciences 10 (2022) 450–455.
[22] P. Wachid, H. Septina, F. Nur Ismi Mustika, K. Kusmardi, D. Ratih Tri Kusuma, P. Santy Ayu Puspita, P. Nurhasan Agung, P. Yeremia Suryo, The effect of Channa striata extract on serum albumin and high sensitive C-reactive protein in end-stage renal disease patients: a randomized controlled trial, Phcog. J. 15 (2023).
[23] U.K. Laemmli, Cleavage of structural proteins during the assembly of the head of bacteriophage T4, Nature 227 (1970) 680–685.
[24] S. Bringans, S. Eriksen, T. Kendrick, P. Gopalakrishnakone, A. Livk, R. Lock, R. Lipscombe, Proteomic analysis of the venom of Heterometrus longimanus (Asian black scorpion), Proteomics 8 (2008) 1081–1096.
[25] A.A. López-Zavala, I.E. Quintero-Reyes, J.S. Carrasco-Miranda, V. Stojanoff, A. Weichsel, E. Rudiño-Piñera, R.R. Sotelo-Mundo, Structure of nucleoside diphosphate kinase from pacific shrimp (Litopenaeus vannamei) in binary complexes with purine and pyrimidine nucleoside diphosphates, Acta Crystallogr F Struct Biol Commun 70 (2014) 1150–1154.
[26] R.Q. Yang, Y.L. Chen, F. Chen, H. Wang, Q. Zhang, G.M. Liu, T. Jin, M.J. Cao, Purification, characterization, and crystal structure of parvalbumins, the major allergens in Mustelus griseus, J. Agric. Food Chem. 66 (2018) 8150–8159.
[27] Y. Zhang, I-TASSER server for protein 3D structure prediction, BMC Bioinf. 9 (2008) 40.
[28] M. Huse, Y.G. Chen, J. Massagué, J. Kuriyan, Crystal structure of the cytoplasmic domain of the type I TGF beta receptor in complex with FKBP12, Cell 96 (1999) 425–436.
[29] C.W. Müller, F.A. Rey, M. Sodeoka, G.L. Verdine, S.C. Harrison, Structure of the NF-kappa B p50 homodimer bound to DNA, Nature 373 (1995) 311–317.
[30] R.A. Laskowski, J. Jabłońska, L. Pravda, R.S. Vařeková, J.M. Thornton, PDBsum: structural summaries of PDB entries, Protein Sci. 27 (2018) 129–134.
[31] C. Dominguez, R. Boelens, A.M.J.J. Bonvin, HADDOCK: a Protein−Protein docking approach based on biochemical or biophysical information, J. Am. Chem. Soc. 125 (2003) 1731–1737.
[32] K.G. Tina, R. Bhadra, N. Srinivasan, PIC: protein interactions calculator, Nucleic Acids Res. 35 (2007) W473–W476.
[33] S. Pronk, S. Páll, R. Schulz, P. Larsson, P. Bjelkmar, R. Apostolov, M.R. Shirts, J.C. Smith, P.M. Kasson, D. van der Spoel, B. Hess, E. Lindahl, Gromacs 4.5: a high-throughput and highly parallel open source molecular simulation toolkit, Bioinformatics 29 (2013) 845–854.
[34] M.J. Robertson, J. Tirado-Rives, W.L. Jorgensen, Improved peptide and protein torsional energetics with the OPLSAA force field, J. Chem. Theor. Comput. 11 (2015) 3499–3509.
[35] Schrödinger, The PyMOL Molecular Graphics System, 2020.
[36] M.S. Valdés-Tresanco, M.E. Valdés-Tresanco, P.A. Valiente, E. Moreno, gmx_MMPBSA: a new tool to perform end-state free energy calculations with GROMACS, J. Chem. Theor. Comput. 17 (2021) 6281–6291.
[37] B.R. Miller 3rd, T.D. McGee Jr., J.M. Swails, N. Homeyer, H. Gohlke, A.E. Roitberg, MMPBSA.py: an efficient program for end-state free energy calculations, J. Chem. Theor. Comput. 8 (2012) 3314–3321.
[38] S.K. Panday, E. Alexov, Protein-protein binding free energy predictions with the MM/PBSA approach complemented with the Gaussian-based method for entropy estimation, ACS Omega 7 (2022) 11057–11067.
[39] T. Wang, B.Y. Li, P.D. Danielson, P.C. Shah, S. Rockwell, R.J. Lechleider, J. Martin, T. Manganaro, P.K. Donahoe, The immunophilin FKBP12 functions as a common inhibitor of the TGF beta family type I receptors, Cell 86 (1996) 435–444.
[40] Y.G. Chen, F. Liu, J. Massague, Mechanism of TGFbeta receptor inhibition by FKBP12, EMBO J. 16 (1997) 3866–3876.
[41] B.R. Stockwell, S.L. Schreiber, TGF-beta-signaling with small molecule FKBP12 antagonists that bind myristoylated FKBP12-TGF-beta type I receptor fusion proteins, Chem Biol 5 (1998) 385–395.
[42] M. Huse, Y.-G. Chen, J. Massagué, J. Kuriyan, Crystal structure of the cytoplasmic domain of the type I TGF β receptor in complex with FKBP12, Cell 96 (1999) 425–436.
[43] C.W. Müller, F.A. Rey, M. Sodeoka, G.L. Verdine, S.C. Harrison, Structure of the NF-κB p50 homodimer bound to DNA, Nature 373 (1995) 311–317.
[44] C.N. Pace, H. Fu, K. Lee Fryar, J. Landua, S.R. Trevino, D. Schell, R.L. Thurlkill, S. Imura, J.M. Scholtz, K. Gajiwala, J. Sevcik, L. Urbanikova, J.K. Myers, K. Takano, E.J. Hebert, B.A. Shirley, G.R. Grimsley, Contribution of hydrogen bonds to protein stability, Protein Sci. 23 (2014) 652–661.
[45] G.G. Ferenczy, M. Kellermayer, Contribution of hydrophobic interactions to protein mechanical stability, Comput. Struct. Biotechnol. J. 20 (2022) 1946–1956.
[46] D. Dermawan, B.A. Prabowo, C.A. Rakhmadina, In silico study of medicinal plants with cyclodextrin inclusion complex as the potential inhibitors against SARS-CoV-2 main protease (Mpro) and spike (S) receptor, Inform. Med. Unlocked 25 (2021) 1–18.
[47] A. Escobedo, B. Topal, M.B.A. Kunze, J. Aranda, G. Chiesa, D. Mungianu, G. Bernardo-Seisdedos, B. Eftekharzadeh, M. Gairí, R. Pierattelli, I.C. Felli, T. Diercks, O. Millet, J. García, M. Orozco, R. Crehuet, K. Lindorff-Larsen, X. Salvatella, Side chain to main chain hydrogen bonds stabilize a polyglutamine helix in a transcription factor, Nat. Commun. 10 (2019) 2034.
[48] A. Bornot, C. Etchebest, A.G. de Brevern, Predicting protein flexibility through the prediction of local structures, Proteins 79 (2011) 839–852.
[49] P. Horx, A. Geyer, Defining the mobility range of a hinge-type connection using molecular dynamics and metadynamics, PLoS One 15 (2020) e0230962.
[50] D. Dhasmana, A. Singh, R. Shukla, T. Tripathi, N. Garg, Targeting nucleotide binding domain of multidrug resistance-associated protein-1 (MRP1) for the reversal of multi drug resistance in cancer, Sci. Rep. 8 (2018).
[51] S. Liang, L. Li, W.L. Hsu, M.N. Pilcher, V. Uversky, Y. Zhou, A.K. Dunker, S.O. Meroueh, Exploring the molecular design of protein interaction sites with molecular dynamics simulations and free energy calculations, Biochemistry 48 (2009) 399–414.
[52] A. Bepari, H. Reza, Identification of a novel inhibitor of SARS-CoV-2 3CL-PRO through virtual screening and molecular dynamics simulation, PeerJ 9 (2021) e11261.
[53] H. Yu, M.J. Wang, N.X. Xuan, Z.C. Shang, J. Wu, Molecular dynamics simulation of the interactions between EHD1 EH domain and multiple peptides, J. Zhejiang Univ. - Sci. B 16 (2015) 883–896.
[54] H. Yu, X. Rao, K. Zhang, Nucleoside diphosphate kinase (Ndk): a pleiotropic effector manipulating bacterial virulence and adaptive responses, Microbiol. Res. 205 (2017) 125–134.

[55] M. Boissan, G. Montagnac, Q. Shen, L. Griparic, J. Guitton, M. Romao, N. Sauvonnet, T. Lagache, I. Lascu, G. Raposo, C. Desbourdes, U. Schlattner, M. L. Lacombe, S. Polo, A.M. van der Bliek, A. Roux, P. Chavrier, Membrane trafficking. Nucleoside diphosphate kinases fuel dynamin superfamily proteins with GTP for membrane remodeling, Science 344 (2014) 1510–1515.
[56] P.S. Chard, D. Bleakman, S. Christakos, C.S. Fullmer, R.J. Miller, Calcium buffering properties of calbindin D28k and parvalbumin in rat sensory neurones, J Physiol 472 (1993) 341–357.
[57] J.Y. Koh, M.B. Wie, B.J. Gwag, S.L. Sensi, L.M. Canzoniero, J. Demaro, C. Csernansky, D.W. Choi, Staurosporine-induced neuronal apoptosis, Exp. Neurol. 135 (1995) 153–159.
[58] T. Wang, P.K. Donahoe, A.S. Zervos, Specific interaction of type I receptors of the TGF-beta family with the immunophilin FKBP-12, Science 265 (1994) 674–676.
[59] T. Yamamoto, N.A. Noble, A.H. Cohen, C.C. Nast, A. Hishida, L.I. Gold, W.A. Border, Expression of transforming growth factor-beta isoforms in human glomerular diseases, Kidney Int. 49 (1996) 461–469.
[60] R.K. Assoian, A. Komoriya, C.A. Meyers, D.M. Miller, M.B. Sporn, Transforming growth factor-beta in human platelets. Identification of a major storage site, purification, and characterization, J. Biol. Chem. 258 (1983) 7155–7160.
[61] M.G. Kazanietz, L.B. Areces, A. Bahador, H. Mischak, J. Goodnight, J.F. Mushinski, P.M. Blumberg, Characterization of ligand and substrate specificity for the calcium-dependent and calcium-independent protein kinase C isozymes, Mol. Pharmacol. 44 (1993) 298–307.
[62] E.N. Baker, R.E. Hubbard, Hydrogen bonding in globular proteins, Prog. Biophys. Mol. Biol. 44 (1984) 97–179.
[63] M.R. Arkin, J.A. Wells, Small-molecule inhibitors of protein-protein interactions: progressing towards the dream, Nat. Rev. Drug Discov. 3 (2004) 301–317.
[64] S. Gross, K. Devraj, Y. Feng, J. Macas, S. Liebner, T. Wieland, Nucleoside diphosphate kinase B regulates angiogenic responses in the endothelium via caveolae formation and c-Src-mediated caveolin-1 phosphorylation, J Cereb Blood Flow Metab 37 (2017) 2471–2484.
[65] B. Schwaller, M. Meyer, S. Schiffmann, 'New' functions for 'old' proteins: the role of the calcium-binding proteins calbindin D-28k, calretinin and parvalbumin, in cerebellar physiology. Studies with knockout mice, Cerebellum 1 (2002) 241–258.
[66] S.E. Bondos, A. Bicknell, Detection and prevention of protein aggregation before, during, and after purification, Anal. Biochem. 316 (2003) 223–231.
[67] H. Jubb, T.L. Blundell, D.B. Ascher, Flexibility and small pockets at protein-protein interfaces: new insights into druggability, Prog. Biophys. Mol. Biol. 119 (2015) 2–9.
[68] Y.H. Yu, D.K. Park, D.Y. Yoo, D.S. Kim, Altered expression of parvalbumin immunoreactivity in rat main olfactory bulb following pilocarpine-induced status epilepticus, BMB Rep 53 (2020) 234–239.
[69] C.W. Heizmann, Parvalbumin, an intracellular calcium-binding protein; distribution, properties and possible roles in mammalian cells, Experientia 40 (1984) 910–921.
[70] M. Koziczak, T. Holbro, N.E. Hynes, Blocking of FGFR signaling inhibits breast cancer cell proliferation through downregulation of D-type cyclins, Oncogene 23 (2004) 3501–3508.
[71] N. Khalil, T.V. Parekh, R. O'Connor, N. Antman, W. Kepron, T. Yehaulaeshet, Y.D. Xu, L.I. Gold, Regulation of the effects of TGF-beta 1 by activation of latent TGF-beta 1 and differential expression of TGF-beta receptors (T beta R-I and T beta R-II) in idiopathic pulmonary fibrosis, Thorax 56 (2001) 907–915.
[72] T. Wang, B.-Y. Li, P.D. Danielson, P.C. Shah, S. Rockwell, R.J. Lechleider, J. Martin, T. Manganaro, P.K. Donahoe, The immunophilin FKBP12 functions as a common inhibitor of the TGFβ family type I receptors, Cell 86 (1996) 435–444.
[73] X. Wang, Z. Zhou, C. Yang, J. Xu, J. Yang, Nuclear factor-κB is involved in the phenotype loss of parvalbumin-interneurons in vitro, Neuroreport 22 (2011) 264–268.
[74] A. Ferro, W. Qu, A. Lukowicz, D. Svedberg, A. Johnson, M. Cvetanovic, Inhibition of NF-κB signaling in IKKβF/F;LysM Cre mice causes motor deficits but does not alter pathogenesis of Spinocerebellar ataxia type 1, PLoS One 13 (2018) e0200013.
[75] Y.J. Kim, J.H. Lee, Y. Lee, J. Jia, S.H. Paek, H.B. Kim, S. Jin, U.H. Ha, Nucleoside diphosphate kinase and flagellin from Pseudomonas aeruginosa induce interleukin 1 expression via the Akt/NF-κB signaling pathways, Infect. Immun. 82 (2014) 3252–3260.
[76] R. Rosyidi, J. Janu, B. Priyanto, A. Islam, M. Hatta, A. Bukhari, The effect of snakehead fish (Channa striata) extract capsule to the albumin serum level of post-operative neurosurgery patients, biomedical and, Pharmacology Journal 12 (2019) 893–899.
[77] F. He, C. Wu, P. Li, N. Li, D. Zhang, Q. Zhu, W. Ren, Y. Peng, Functions and signaling pathways of amino acids in intestinal inflammation, BioMed Res. Int. 2018 (2018) 9171905.
[78] H. Moshage, Cytokines and the hepatic acute phase response, J. Pathol. 181 (1997) 257–266.
[79] M.H. Park, J.T. Hong, Roles of NF-κB in cancer and inflammatory diseases and their therapeutic approaches, Cells 5 (2016).
[80] T. Liu, L. Zhang, D. Joo, S.C. Sun, NF-κB signaling in inflammation, Signal Transduct Target Ther 2 (2017) 17023.
[81] R.H. Shih, C.Y. Wang, C.M. Yang, NF-kappaB signaling pathways in neurological inflammation: a mini review, Front. Mol. Neurosci. 8 (2015) 77.
[82] V. Arroyo, R. García-Martinez, X. Salvatella, Human serum albumin, systemic inflammation, and cirrhosis, J. Hepatol. 61 (2014) 396–407.
[83] S. Yuli, H. Suharyo, N. Sri Achadi, The effect of snakehead fish (Channa striata) extract on blood leukocyte number and cesarean section wound healing. Proceedings of the International Conference on Science and Education and Technology (ISET 2019), Atlantis Press, 2020, pp. 596–598.
[84] N. Paliliewu, E. Datau, J. Matheos, E. Surachmanto, Channa striatus capsules induces cytokine conversion in pulmonary tuberculosis patients, J. Exp. Integr. Med. 3 (2013) 1.
[85] Z.-p. Wang, S.-x. Cai, D.-b. Liu, X. Xu, H.-p. Liang, Anti-inflammatory effects of a novel peptide designed to bind with NF-κB p50 subunit, Acta Pharmacol. Sin. 27 (2006) 1474–1478.
[86] S. Chakrabarti, F. Jahandideh, J. Wu, Food-derived bioactive peptides on inflammation and oxidative stress, BioMed Res. Int. 2014 (2014) 608979.